Current Topics（カレントトピックス）

Shimakami, T. et al.：Proc. Natl. Acad. Sci. USA, 109：941-946, 2012

miR-122－Ago2複合体による C型肝炎ウイルスRNAの安定化

島上哲朗，山根大典，Stanley M. Lemon

肝臓特異的なマイクロRNAであるmiR-122は，C型肝炎ウイルス（HCV）の複製を促進することが知られていたが，その分子機構は不明であった．今回われわれは，miR-122がHCV RNAの5′末端に結合することでHCV RNAを安定化すること，さらにその安定化にはAgo2（Argonaute 2）が必須であることを明らかにした．

C型肝炎ウイルス（HCV）は，約9.6 kbの一本鎖＋鎖RNAウイルスで，C型慢性肝炎，肝硬変，肝がんの原因である．一方miR-122は，肝臓特異的なmiRNA（マイクロRNA）であり，肝臓内miRNAの約60％を占めている．Sarnowらのグループは，HCVの5′非翻訳領域（UTR）にmiR-122結合部位が2カ所存在し，miR-122はHCV 5′UTRとの結合を介してHCV複製を促進することを報告した（図1 A）[1]～[3]．またLanfordらは，HCV感染チンパンジーにmiR-122を阻害するアンチセンス鎖を投与し，その強力な抗ウイルス効果を報告した[4]．そのためmiR-122は抗HCV薬の有力な標的として注目されている．一般にmiRNAは，細胞mRNAの3′UTR領域に結合し標的タンパク質発現を抑制するため，miR-122によるHCV複製の促進はmiRNAの機能としてはきわめてユニークなものである．その後miR-122はHCVのIRES（internal ribosome entry site）依存性のタンパク質翻訳を促進することが報告されたが[5]，その詳細な分子機構は不明であった．今回われわれはmiR-122がHCV RNAを安定化することでタンパク質発現を促進し，その安定化にAgo2（Argonaute 2）が必須であることを明らかにした．

miR-122は細胞内に導入したHCV RNAを安定化することでタンパク質発現を促進する

まずわれわれは，miR-122のHCV RNAへの安定性とタンパク質発現に対する影響とを同時に検討するため，HCVのp7（ウイルス粒子の構造タンパク質の1つ）と非構造タンパク質NS2との間にGLuc（*Gaussia* luciferase）と口蹄疫ウイルスの2A配列（FMDV2A）を挿入した．GLucはFMDV2Aの自己プロテアーゼ活性による切断を受け，自身の分泌シグナル依存的に細胞外へ分泌されることから，細胞上清中のGLuc活性を測定することでウイルスタンパク質発現を定量した．さらにmiR-122のHCV RNA複製に対する影響を除外するため，HCVのRNA複製酵素NS5Bの活性中心GDDを不活性のAAGに置換したHCV RNAを実験に

Stabilization of hepatitis C virus RNA by an Ago2-miR-122 complex

Tetsuro Shimakami[1]/Daisuke Yamane[2]/Stanley M. Lemon[2]：Department of Disease Control and Homeostasis, Division of Environmental Science, Kanazawa University Graduate School of Medical Science[1]/Lineberger Comprehensive Cancer Center and Division of Infectious Diseases, Department of Medicine, University of North Carolina at Chapel Hill[2]（金沢大学大学院医学系研究科環境医科学専攻恒常性制御学講座[1]/ノースカロライナ大学チャペルヒル校医学部ラインバーガー総合がんセンター[2]）

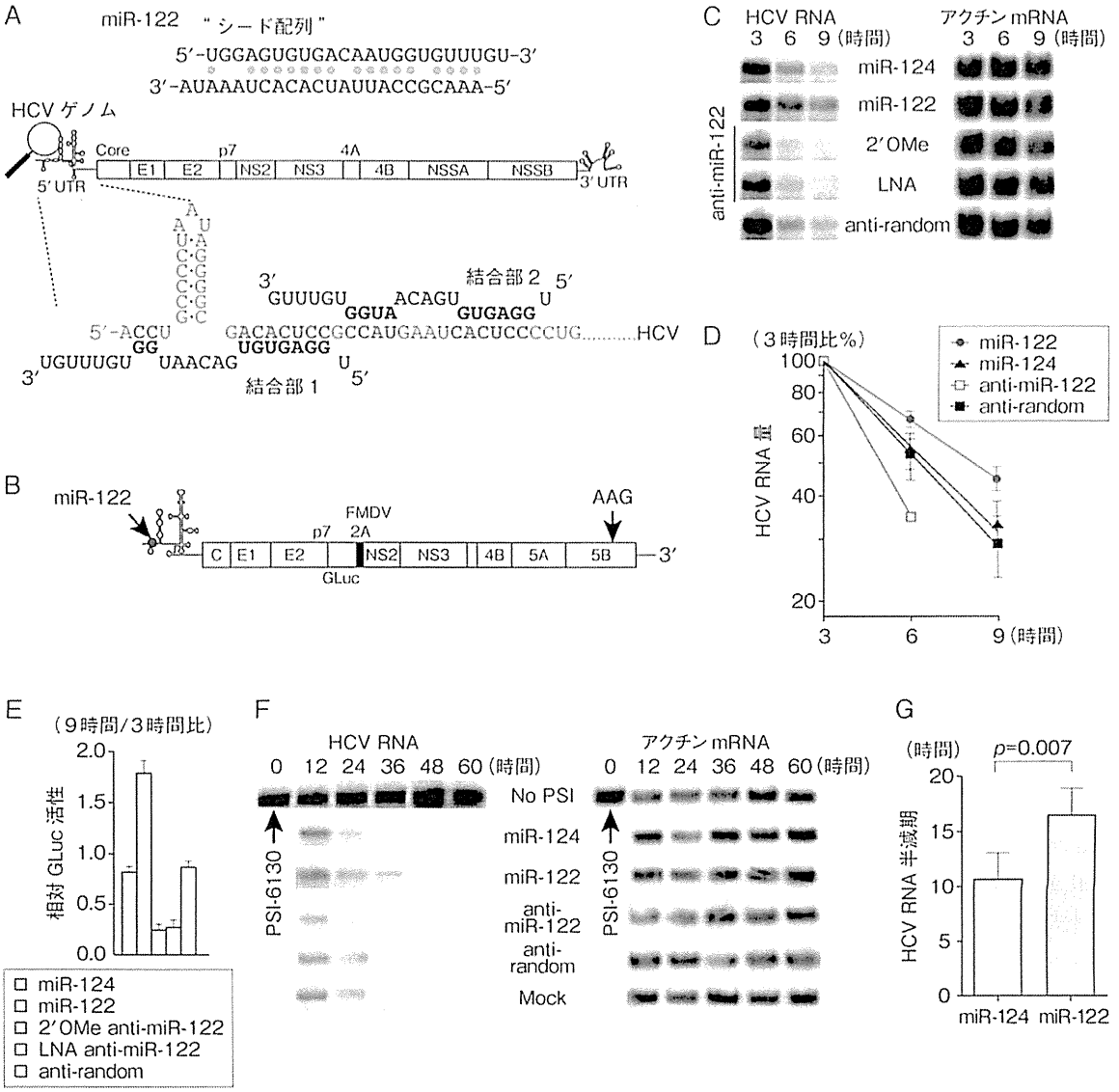

図1　miR-122は，HCV RNAを安定化する

A) HCVゲノムとmiR-122．HCVは5′UTRに2カ所のmiR-122結合部位を有する．B) GLucを含んだ非複製HCV RNA，H77S/GLuc2A/AAG．p7とNS2の間にGLuc，FMDV2A配列を挿入し，NS5Bの活性中心GDDを不活性のAAGに置換した．C) miR-122およびアンチセンス鎖（anti-miR-122）のHCV RNAの安定性に対する影響．H77S/GLuc2A/AAGを図に示すmiRNAまたは一本鎖RNAとともにエレクトロポレーションにより細胞内導入し，3時間おきに細胞トータルRNAを回収した後，HCV RNAとアクチンmRNAをノーザンブロット法により定量した．D) miR-122のHCV RNAの安定性に対する影響．Cの結果を定量し，3時間値に対するHCV RNAの減衰を示す．E) miR-122のHCV RNAのタンパク質翻訳に対する影響．H77S/GLuc2A/AAGを，図に示すmiRNAまたは一本鎖RNAとともに細胞内導入し，3時間おきに細胞上清を回収後GLuc活性を測定し，9時間値を3時間値で補正した．F) miR-122の持続感染細胞内HCV RNAの安定性に対する影響．HCV持続感染細胞にNS5B阻害剤PSI-6130を投与し，RNA複製を抑制した状態で，図に示すmiRNAまたは一本鎖RNAを導入し，細胞トータルRNAを12時間おきに回収した後，HCV RNAとアクチンmRNAをノーザンブロット法により定量した．G) HCV持続感染細胞におけるmiR-122によるHCV RNA半減期の延長．Fを定量し，算出した（文献6より転載）

用いた（H77S/GLuc2A/AAG，図1B）．この複製能を有しないHCV RNAをmiR-122あるいは2種類のmiR-122に対するアンチセンス鎖（anti-miR-122，2′O-methyl：2′OMe，locked nucleic acid：LNA修飾）とともに肝がん細胞株Huh-7細胞にエレクトロポレーションにより導入し，細胞トータルRNAと細胞上清の回収を3時間間隔で9時間後まで行った．脳特異的なmiRNAであるmiR-124と，いずれのmiRNAとも結合しない一本鎖RNA（anti-random）をコントロールとして用いた．HCV RNAの安定性に関しては，HCVに対するプローブを用いてノーザンブロット解析により評価した．図1C，Dに示すようにmiR-122はmiR-124に比べてHCV RNAを安定化し，逆にanti-miR-122はanti-randomに比べてHCV RNAを不安定化した．同時に細胞上清中のGLuc活性を測定したところ，miR-122とanti-miR-122のGLuc活性への影響はHCV RNAの安定性に対する影響とほぼ同一であった（図1E）．これらの結果からmiR-122はHCV RNAの安定性を増加させることでHCVタンパク質発現を促進していることが明らかとなった．

miR-122はHCV持続感染細胞においてもHCV RNAを安定化する

前述の結果は，非複製HCV RNAを用いている点，また大量の合成HCV RNAを細胞内に導入している点で非生理的である．細胞内で持続的に複製しているHCV RNAと非複製HCV RNAの分解経路は異なる可能性が考えられたことから，HCV持続感染細胞を作成し，複製HCV RNAに対するmiR-122の影響を検討した．miR-122のHCV RNA合成に対する影響を除外するため，NS5B特異的阻害剤PSI-6130を半有効濃度の約10倍量でHCV持続感染細胞に投与し，HCV RNA合成を停止させた．同時にmiR-122，anti-miR-122およびコントロールを投与し，12時間間隔で60時間後まで細胞トータルRNAを回収し，ノーザンブロット解析によってHCV RNAの安定性を評価した（図1F：ノーザンブロット，G：HCV RNA半減期）．その結果HCV感染細胞においてもmiR-122は有意にHCV RNAを安定化し半減期を延長することが明らかとなった．

miR-122はAgo2とともにHCV RNAとの複合体を形成する

一般にsiRNAやmiRNAなどのスモールRNAは，それ自身が単独で働くのではなく，RNA誘導サイレンシング複合体（RISC）と複合体を形成することにより，はじめて標的遺伝子の発現を制御する．そこでまずHCV持続感染細胞を用い，RISCの主要コンポーネントであるAgo1-4がHCV複製に与える影響を検討した．siRNAを用いて，Ago1-4およびmiRNAの生合成に関与するDicerをそれぞれノックダウンし，HCV RNA量を定量RT-PCRを用いて測定したところ（図2A），Ago2ノックダウンのみにおいて HCV複製が抑制された．このことから，Ago2がmiR-122を介してHCV RNAと複合体を形成している可能性を免疫沈降法により検証した．miR-122をもたないマウス胎仔線維芽細胞（MEF）にHCV RNAとmiR-122をエレクトロポレーションにより導入し，導入後6時間のライセート中のAgo2を特異的抗体により免疫沈降し，Ago2複合体中のHCV RNAの有無をRT-PCR法にて検出した．また，配列特異的な相互作用の有無を検討するため，HCV 5′UTRの2カ所のmiR-122結合部位に点変異をもちmiR-122と結合しないHCV RNA（p6m）と，p6mとの結合能を有する変異体miR-122（miR-122p6）を作成した．コントロールIgGを用いて免疫沈降した際は，HCV RNAは検出されなかったが（図2B左），Ago2抗体を用いた際はHCV RNAとmiR-122の結合特異的なHCV RNAの存在が認められた（図2B右）．以上の結果から，Ago2はmiR-122を介してHCV RNAと複合体を形成することが明らかとなった．

HCV RNAの安定化にはAgo2が必須である

次にmiR-122のHCV安定化機能に対するAgo2の役割をAgo2ノックアウトマウス由来MEFを用いて検討した．H77S/GLuc2A/AAG RNAをmiR-122あるいはmiR-124とともにAgo2ノックアウトおよび野生型MEFにエレクトロポレーションにて導入し，細胞トータルRNAと細胞上清の回収を3時間間隔で行い，それぞれノーザンブロットおよびGLuc活性の測定を行なった．miR-122は野生型MEFではHCV RNAを安定化したが（図2C上段），Ago2ノックアウトMEF

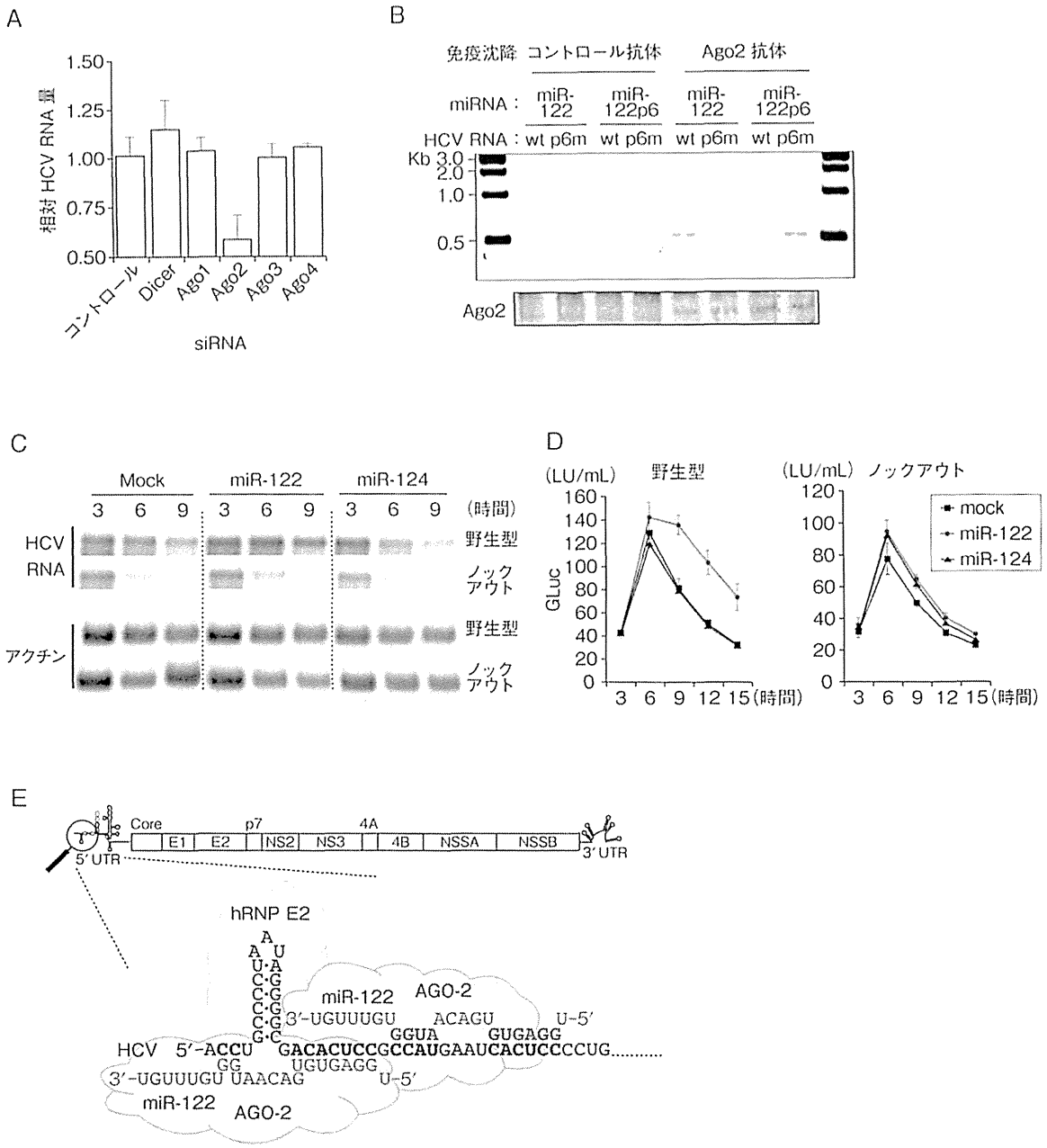

図2 miR-122によるHCV RNAの安定化にはAgo2が必須である

A) HCV複製に対するRNA誘導サイレンシング複合体（RISC）関連タンパク質の影響．HCV持続感染細胞に図に示すsiRNAを導入し，HCV複製に対する影響を定量RT-PCRを用いて評価した．B) miR-122を介したHCV RNAとAgo2との複合体形成．マウス胎仔線維芽細胞（MEF）にmiR-122とHCV RNAを導入し，特異的モノクローナル抗体を用いてAgo2を免疫沈降後，HCV RNAの有無をRT-PCR法にて検出した．p6mは，HCV RNAの5′UTRに存在する2カ所のmiR-122結合部位に結合能を欠損させる点変異を含んだ変異体で，miR-122p6は，p6mとの結合能を有する変異型miR-122．C) Ago2のmiR-122によるHCV RNA安定化機能に対する役割．Ago2ノックアウトおよび野生型MEFに，図に示すmiRNAをH77S/GLuc2A/AAGとともに導入し，細胞トータルRNAを3時間おきに回収した後，HCV RNAとActin mRNAをノーザンブロット法により検出した．D) Ago2のmiR-122によるHCV RNAのタンパク質翻訳に対する影響．Ago2ノックアウトおよび野生型MEFに，図に示すmiRNAをH77S/GLuc2A/AAGとともに導入し，細胞上清を3時間おきに回収し，GLuc活性を測定した．E) miR-122とAgo2によるHCV 5′末端での複合体形成の模式図（文献6，7より転載）

ではHCV RNAを安定化しなかった（図２C下段）．同時に，タンパク質発現への影響をGLuc活性測定によって検討したところ，miR-122は野生型MEFではタンパク質発現を促進したが（図２D左），Ago2ノックアウトMEFではタンパク質発現に影響を与えなかった（図２D右）．この結果からAgo2がmiR-122によるHCV RNAの安定化のエフェクター分子であると考えられた．

おわりに

一般にmRNAの５′末端に存在するcap構造は，mRNAを５′-エキソヌクレアーゼによる分解から保護することが知られている．HCV RNAの５′末端にcap構造を付加して保護した場合，miR-122によるHCV RNA安定化作用は認められなかった[6]．この結果は，HCV RNAの５′末端に結合したmiR-122は，Ago2や他のタンパク質（hRNP E2など）とともに複合体を形成し，５′-エキソヌクレアーゼによる分解から保護していると考えられる（図２E）．Ago2はAgo1-4タンパク質のなかで唯一標的RNAを切断する活性を有し，miRNAによる標的遺伝子抑制のキータンパク質と考えられている．今回われわれは，miR-122がHCV RNAの５′末端にAgo2を含むタンパク質複合体をリクルートすることでその半減期を延長することを明らかにしたが，Ago2が一般的に知られている機能とは逆に標的RNAを安定化する機序は不明であり，今後のさらなる検討が必要である．

文献

1）Jopling, C. L. et al.：hepatitis C virus RNA abundance by a liver-specific MicroRNA. Science, 309：1577-1581, 2005
2）Jopling, C. L. et al.：Position-dependent function for a tandem microRNA miR-122-binding site located in the hepatitis C virus RNA genome. Cell Host Microbe, 17：77-85, 2008
3）Machlin, E. S. et al.：Masking the 5′terminal nucleotides of the hepatitis C virus genome by an unconventional microRNA-target RNA complex. Proc. Natl. Acad. Sci. USA, 108：3193-3198, 2011
4）Lanford, R. E. et al.：Therapeutic silencing of microRNA-122 in primates with chronic hepatitis C virus infection. Science, 327：198-201, 2010
5）Henke, J. I. et al.：microRNA-122 stimulates translation of hepatitis C virus RNA. EMBO J, 27：3300-3310, 2008
6）Shimakami, T. et al.：Stabilization of hepatitis C virus RNA by an Ago2-miR-122 complex. Proc. Natl. Acad. Sci. USA, 109：941-946, 2012
7）Shimakami, T. et al.：Base-pairing between Hepatitis C Virus RNA and miR-122 3′of its Seed Sequence is Essential for Genome Stabilization and Production of Infectious Virus. J. Virol. in press（2012）

● 筆頭著者プロフィール ●

島上哲朗：1998年，金沢大学医学部卒業，2004年，同大学大学院医学系研究科修了．2008年から米テキサス大学（ガルベストン校），'10年より米ノースカロライナ大学（チャペルヒル校）留学，'11年４月より金沢大学付属病院恒常性制御学講座にて，患者診療，および肝炎，肝がんの基礎研究を行なっている．

SCIENTIFIC REPORTS

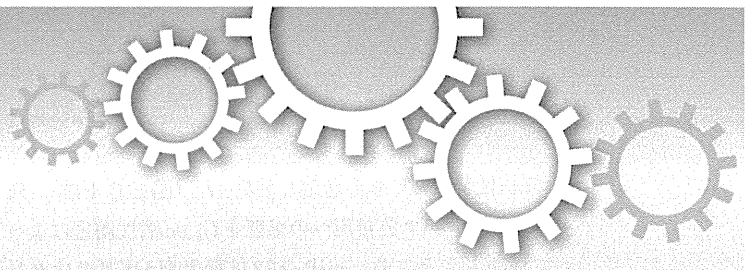

OPEN

SUBJECT AREAS:
HEPATITIS B VIRUS
HEPATITIS C VIRUS
TRANSCRIPTOMICS
CANCER GENOMICS

Received
8 August 2014

Accepted
5 December 2014

Published
8 January 2015

Small tRNA-derived RNAs are increased and more abundant than microRNAs in chronic hepatitis B and C

Sara R. Selitsky[1,2,3,4], Jeanette Baran-Gale[1,2], Masao Honda[5], Daisuke Yamane[3,4], Takahiro Masaki[3,4], Emily E. Fannin[2], Bernadette Guerra[6], Takayoshi Shirasaki[5], Tetsuro Shimakami[5], Shuichi Kaneko[5], Robert E. Lanford[6], Stanley M. Lemon[3,4]* & Praveen Sethupathy[1,2,4]*

[1]Bioinformatics and Computational Biology Curriculum, University of North Carolina at Chapel Hill, Chapel Hill, North Carolina, United States of America, [2]Department of Genetics, University of North Carolina at Chapel Hill, Chapel Hill, North Carolina, United States of America, [3]Departments of Medicine and Microbiology & Immunology, University of North Carolina at Chapel Hill, Chapel Hill, North Carolina, United States of America, [4]Lineberger Comprehensive Cancer Center, University of North Carolina at Chapel Hill, Chapel Hill, North Carolina, United States of America, [5]Department of Gastroenterology, Kanazawa University Graduate School of Medicine, Kanazawa, Japan, [6]Department of Virology and Immunology, Texas Biomedical Research Institute and Southwest National Primate Research Center, San Antonio, Texas, United States of America.

Correspondence and requests for materials should be addressed to P.S. (praveen_sethupathy@med.unc.edu)

* These authors contributed equally to this work

Persistent infections with hepatitis B virus (HBV) or hepatitis C virus (HCV) account for the majority of cases of hepatic cirrhosis and hepatocellular carcinoma (HCC) worldwide. Small, non-coding RNAs play important roles in virus-host interactions. We used high throughput sequencing to conduct an unbiased profiling of small (14-40 nts) RNAs in liver from Japanese subjects with advanced hepatitis B or C and hepatocellular carcinoma (HCC). Small RNAs derived from tRNAs, specifically 30–35 nucleotide-long 5′ tRNA-halves (5′ tRHs), were abundant in non-malignant liver and significantly increased in humans and chimpanzees with chronic viral hepatitis. 5′ tRH abundance exceeded microRNA abundance in most infected non-cancerous tissues. In contrast, in matched cancer tissue, 5′ tRH abundance was reduced, and relative abundance of individual 5′ tRHs was altered. In hepatitis B-associated HCC, 5′ tRH abundance correlated with expression of the tRNA-cleaving ribonuclease, angiogenin. These results demonstrate that tRHs are the most abundant small RNAs in chronically infected liver and that their abundance is altered in liver cancer.

Hepatitis B virus (HBV) and hepatitis C virus (HCV) are phylogenetically unrelated non-cytopathic viruses that infect the liver[1]. While HBV is a DNA virus, and HCV is a positive-strand RNA virus, both have the capacity to persist for years in some infected individuals. Hundreds of millions of people worldwide are chronic carriers of HBV or HCV, 30–50% of whom have chronic liver disease[2]. Together, these viral infections are responsible for ~60% of liver cirrhosis and ~80% of hepatocellular carcinoma (HCC), a leading cause of cancer-related deaths worldwide. Numerous studies suggest that microRNAs (miRNAs), small 21–23 nt non-coding RNAs are important in the pathogenesis of these infections, modulating viral replication as well as host responses and possibly influencing the risk of carcinogenesis[3]. For example the HBV X protein represses expression of miR-148a, potentially enhancing tumorigenesis[4]. In contrast, HCV infection is associated with higher expression of miR-21, which targets key components of Toll-like receptor signaling pathways, possibly facilitating viral evasion of innate immune responses[5]. miR-122 stabilizes HCV RNA and promotes its replication[6,7], and the importance of this interaction is reflected in the clinical development of an anti-miR-122 antagomir (miravirsen) as an antiviral therapeutic[8].

Somewhat larger, 30–35 nt RNAs derived from the 5′ half of tRNA (5′ tRHs) represent a second major class of small non-coding RNA[9]. Increased expression of 5′ tRHs has been associated with viral and rickettsial infections in animals[10,11], and may serve to prevent apoptosis and promote cell survival[12]. However, they have not been studied previously in the context of viral hepatitis. To our knowledge, only one study has described unbiased profiling of small RNAs in the liver during chronic viral hepatitis[13], but the analysis was restricted to miRNAs. We sequenced small (14–40 nts) RNAs in liver biopsies from subjects with chronic hepatitis and HCC, examining both non-tumor and matched cancer tissue, and found a surprisingly high proportion of reads representing 5′ tRHs[9]. Our results document their presence in human tissue, demonstrate that they are the most highly abundant

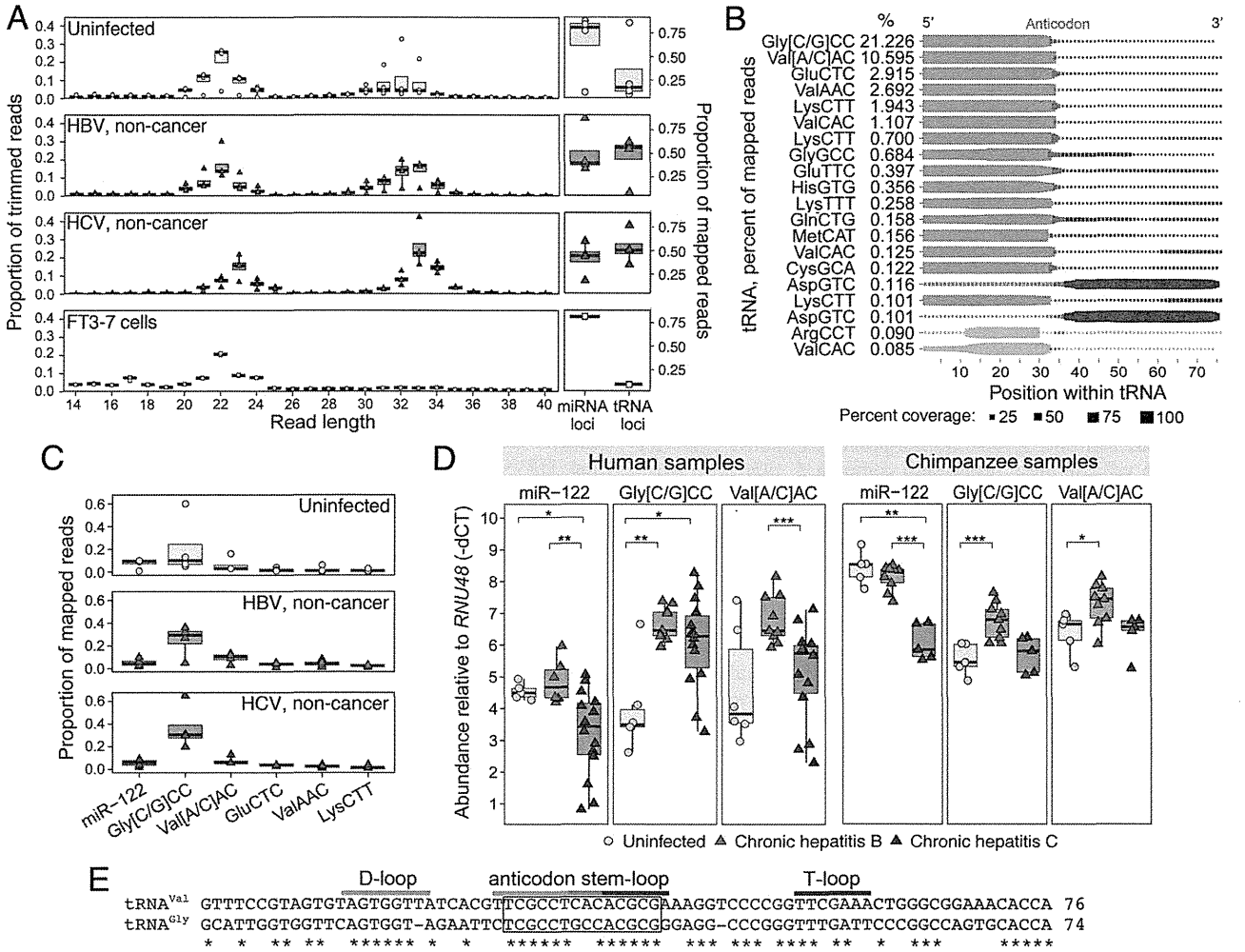

Figure 1 | tRH abundance in HBV- and HCV-infected liver. (a) (left) Read length distribution of 14–40 nt RNAs in non-malignant liver from uninfected, HBV-, or HCV-infected subjects (n=4 each), and FT3-7 cells (n=3 replicates). (right) Proportion of reads mapping to miRNA versus tRNA loci. Boxes represent median ± 1.5 * interquartile range. (b) tRNA coverage plot from the average of the 20 non-cancer samples. Dot size represents percent of reads mapping at each base position within each tRNA (top 20 by average abundance). The anticodon is red, with 5′ bases green and 3′ bases blue. Gray: bases of RNAs that are non-tRHs. See Supplemental Figure 1. (c) Proportion of mapped reads aligning to miR-122 versus the five most abundant tRNA-derived RNAs. (d) (left) Expression levels (RT-qPCR) of miR-122, 5′ tRH^{Gly} ("Gly[C/G]CC") and 5′ tRH^{Val} ("Val[A/C]AC") in uninfected (n=5–6), HBV-infected (n=6–9) and HCV-infected (n=14) human liver. Numbers of samples differ due to limited RNA. (right) Similar results from uninfected (n=5), HBV-infected (n=9), and HCV-infected C (n=5) chimpanzees. *RNU48* was used as a normalizer. *P < 0.05; **P < 0.01; ***P < 0.005 by Mann-Whitney U-test. (e) ClustalW[43] multiple sequence alignment of representative tRNA^{Gly} and tRNA^{Val} genes from which 5′ tRH^{Gly} and 5′ tRH^{Val} could originate (see Supplemental Figure 3). tRNAs regions are highlighted according to the color scheme in panel (b). The box identifies a unique conserved sequence motif described in the text. "Mapped reads" represents all reads aligning to miRNAs or tRNAs (see Methods).

small RNAs in virus-infected liver, and show that their abundance is altered in various disease states including hepatocellular carcinoma.

Results

tRNA-half abundance is significantly increased in chronic viral hepatitis. We employed high-throughput sequencing to characterize the small RNA transcriptome in liver tissue from Japanese adults with advanced hepatitis B or hepatitis C and concomitant HCC (see Supplemental Table 1 for patient information; see Supplemental Tables 2–4 for summary statistics on RNA, qRT-PCR, and sequencing). Initial studies focused on non-malignant tissue from 4 subjects with hepatitis B (mean age 53 ± 4 yrs s.e.m.), 4 with hepatitis C (63 ± 2 yrs), and 4 uninfected individuals undergoing resection of metastatic tumors (60 ± 10 yrs)[14]. A large proportion of the sequencing reads were 19–25 nts in length (median 38%, range 10–73%), as expected for miRNAs[15] (Figure 1a, left). However, we detected an equal or greater abundance of 30–35 nt reads in HBV- and HCV-infected liver (median 54%, range 14–80%). These larger RNAs were less abundant in uninfected tissue (median 21%, range 14–84%) and in human hepatoma (FT3-7) cells (median 9%, range 8.7–9.3%).

Most (~65%) of the 30–35 nt reads in infected samples aligned perfectly to the region 5′ of the anticodon triplet in annotated tRNA genes[16] (Figure 1b, Supplemental Figure 1, Supplemental Table 5 and 6). We refer to these as "5′ tRNA-halves" (5′ tRHs)[9]. Many of the remaining 30–35 nt reads also aligned to the 5′ end of tRNAs, particularly tRNA^{Gly}, but with one or more nucleotide deletions. Also present were 3′ tRHs (~36–39 nts) mapping to the region 3′ of the anticodon, including the 3′ terminal CCA (Figure 1b, Supplemental Figure 1). Additionally, we identified shorter reads derived from 3′ or 5′ tRNA termini, referred to previously as "tRNA fragments"[9] (tRFs), or the region immediately 5′ or 3′ of the anticodon loop, but these

were much less frequent. In 6 of 8 infected livers, more reads mapped to tRNA loci[16] than to known miRNAs[17] (see Methods), while the opposite was true in 3 of 4 uninfected tissues as well as FT3-7 cells (Figure 1a, right).

There are 625 annotated tRNA genes in the human genome (hg19) encoding 458 unique tRNA sequences. We identified reads mapping to 348 of these 458 sequences. Notably, in 11 of the 12 subjects, the same five 5′ tRHs comprised >80% of tRNA-derived reads (Supplemental Figure 2a). The two most abundant 5′ tRHs were Gly[C/G]CC ("5′ tRH^{Gly}"), which could be derived from any of 10 $tRNA^{Gly}$ genes with identical 5′ sequence, and Val[A/C]AC ("5′ tRH^{Val}"), which could originate from any of 15 $tRNA^{Val}$ genes (Figure 1b and C, Supplemental Figure 1 and 3, and Supplemental Table 5)[16]. 5′ tRH^{Gly} accounted for 54 ± 9% (s.d.) and 5′ tRH^{Val} 17 ± 9% of all tRNA-derived RNA reads (Supplemental Figure 2a). Remarkably, 5′ tRH^{Gly} abundance exceeded that of miR-122, one of the most abundant liver miRNAs[13], in 7 of 8 virus-infected tissues.

We used real-time reverse transcription quantitative PCR (RT-qPCR) to validate these results and compare 5′ tRH^{Gly}, 5′ tRH^{Val} and miR-122 abundance in liver tissue from 22 additional subjects (Supplemental Table 1–3)[14]. These analyses confirmed that 5′ tRH^{Gly} abundance was increased in HBV- and HCV-infected liver compared with uninfected tissues ($P<0.01$ and $P<0.05$, respectively) (Figure 1d, left). A similar trend was observed for 5′ tRH^{Val} (HBV $P=0.07$; HCV $P=0.7$). 5′ tRH^{Gly} and 5′ tRH^{Val} were more abundant than miR-122 in HBV- and HCV-infected liver (5′ tRH^{Gly}, $P<0.005$ for both HBV and HCV; 5′ tRH^{Val}, $P<0.005$ for HBV and $P<0.01$ for HCV) (Figure 1d left). Notably, 5′ tRH^{Val} abundance was higher in HBV- than in HCV-infected tissues ($P<0.005$).

Chimpanzees (*Pan troglodytes*) recapitulate many aspects of HBV and HCV infections in humans[18,19], and are free of potential confounding variables (e.g., alcohol intake, smoking) that are difficult to control in human cohorts. Similar to humans, we found that intrahepatic 5′ tRH^{Gly} and 5′ tRH^{Val} abundance was increased in archived liver tissue from chimpanzees chronically infected with HBV compared to uninfected animals ($P<0.005$ and $P<0.05$, respectively) (Figure 1d, right, and Supplemental Table 7). However, 5′ tRH abundance was not increased in chronically HCV-infected chimpanzee liver.

In human tissues, the relative abundance of specific tRNA-derived RNAs correlated with codon usage (codon frequency in DNA sequence) (Spearman's $rho=0.32$, $P=0.01$) and the number of possible tRNA genes from which each could originate ($rho=0.41$, $P=0.001$) (Supplemental Figure 2b). However, tRNAs representing potential sources of the five most abundant tRHs were not the most highly ranked by gene number or codon usage, suggesting that additional factors likely determine tRH biogenesis (Supplemental Figure 4). Interestingly, those tRNAs from which 5′ tRH^{Gly} and 5′ tRH^{Val} are potentially derived share a unique sequence motif in the anticodon stem-loop region (Figure 1e) not present in other tRNAs (Supplemental Figure 3).

tRNA-half abundance is altered in viral hepatitis associated cancer. In HCC tissue from HBV-infected subjects, RT-qPCR analysis showed that 5′ tRH^{Gly} and 5′ tRH^{Val} abundance was significantly reduced ($P<0.005$ for both) (Figure 2a). Similar reductions were evident in HCV-associated cancer tissue, but significant only for 5′ tRH^{Val} ($P<0.05$). We then sequenced small RNAs in cancer tissue from 4 HBV- and 4 HCV-infected subjects. The proportion of reads mapping to tRNA genes was reduced in 4 of 7 samples for which a paired analysis with non-malignant liver was possible, and relatively unchanged in the other 3 (Figure 2b). Although tRNA-derived RNA expression profiles were similar across non-malignant tissues from different subjects, there was substantial variation when compared to cancer tissues (Figure 2c). This suggests that the relative abundance of specific tRNA-derived RNAs is altered in HCC. Notably, the relative abundance of 5′ tRH^{Gly} was reduced by ~50–60% in both HBV- and HCV-associated cancer (Figure 2d).

tRNA-half abundance correlates with angiogenin levels in HBV-associated cancer. Angiogenin (encoded by the gene *ANG*) is best known for its role in angiogenesis, but several studies suggest its RNase activity contributes to tRH biogenesis[20,21]. Consistent with this, analysis of previous microarray data obtained from these tissues[14] revealed that *ANG* mRNA was reduced in both HBV- and HCV-associated cancer compared to non-malignant tissue ($P<0.01$ and $P<0.005$, respectively) or uninfected liver ($P<0.005$ and $P=0.01$) (Figure 3a). Analysis of data from The Cancer Genome Atlas (https://tcga-data.nci.nih.gov/tcga/) also indicates that *ANG* expression is reduced in HCC compared to non-malignant tissue, although the difference is significant only for HBV-associated cancer (HBV $P<0.005$, HCV $P=0.12$) (Supplemental Figure 5). *ANG* mRNA abundance correlated strongly with 5′ tRH expression in the HBV-infected subjects we studied (5′ tRH^{Gly}: Spearman's $rho=0.67$, $P<0.01$; 5′ tRH^{Val}: $rho=0.74$, $P<0.005$) (Figure 3b). Quantitative immunoblot analyses (Supplemental Figure 6) confirmed a correlation between ANG protein abundance and 5′ tRH expression in HBV-associated cancer (5′ tRH^{Gly}: $rho=0.83$, $P<0.005$; 5′ tRH^{Val}: $rho=0.87$, $P<0.005$) (Figure 3c). ANG was expressed within the cytoplasm of hepatocytes (Figure 3d), and although its expression varied substantially in different tumors (Figure 3e), reductions in ANG expression likely explain the reduced tRH abundance we observed in most HBV-associated cancers. Unfortunately, however, the available tissue sections from these subjects were insufficient to power a formal analysis of the correlation between cytoplasmic versus nuclear expression of ANG and tRH abundance. ANG expression correlated poorly with tRH abundance in HCV-infected livers, suggesting that other factors determine tRH biogenesis.

Discussion

Recent advances in high-throughput sequencing technology have unveiled the complexity and diversity of functional small RNAs. We found that small RNAs derived from tRNAs, specifically 5′ tRNA-halves[9] (5′ tRHs, ~30–35 nts), are abundant in liver, significantly increased during chronic viral infection, and altered in abundance in liver cancer associated with these infections. We do not believe that these tRNA-halves are products of stochastic endonuclease cleavage of tRNAs for several reasons. First, the same tRNA-halves were found to be increased in chronic viral hepatitis across all individuals. Second, each tRNA-half family exhibited a uniform length distribution (e.g., 5′ tRH^{Gly} was represented primarily by reads of length 32–34 in every individual). Third, tRNA-halves were preferentially induced in chronic HBV infection (as compared to chronic HCV infection) in both human and chimpanzee tissue, indicating biological specificity. Finally, tRH abundance was correlated with disease state (cancer versus non-cancer), indicating reproducible sensitivity to the cellular environment.

Several models of disease have been shown to exhibit an increase in tRH abundance, including cultured human airway cells infected with respiratory syncytial virus[22], mice infected with spotted-fever group rickettsia[23], and rats treated with cisplatin[24]. While their function is not well understood, previous work in cell culture suggests that some tRHs promote cell survival, are anti-apoptotic[12], reduce translation[25], and promote the formation of stress granules[26]. Preliminary studies in our laboratory do not support a role for 5′ tRH^{Gly} or 5′ tRH^{Val} in the regulation of global protein translation in human hepatoma cells (Supplemental Figure 7–8); however, more detailed investigation is required to uncover the potential functions of tRHs. It has also been suggested that tRHs may alter the immune response due to their enrichment in mouse lymphoid organs[27], high

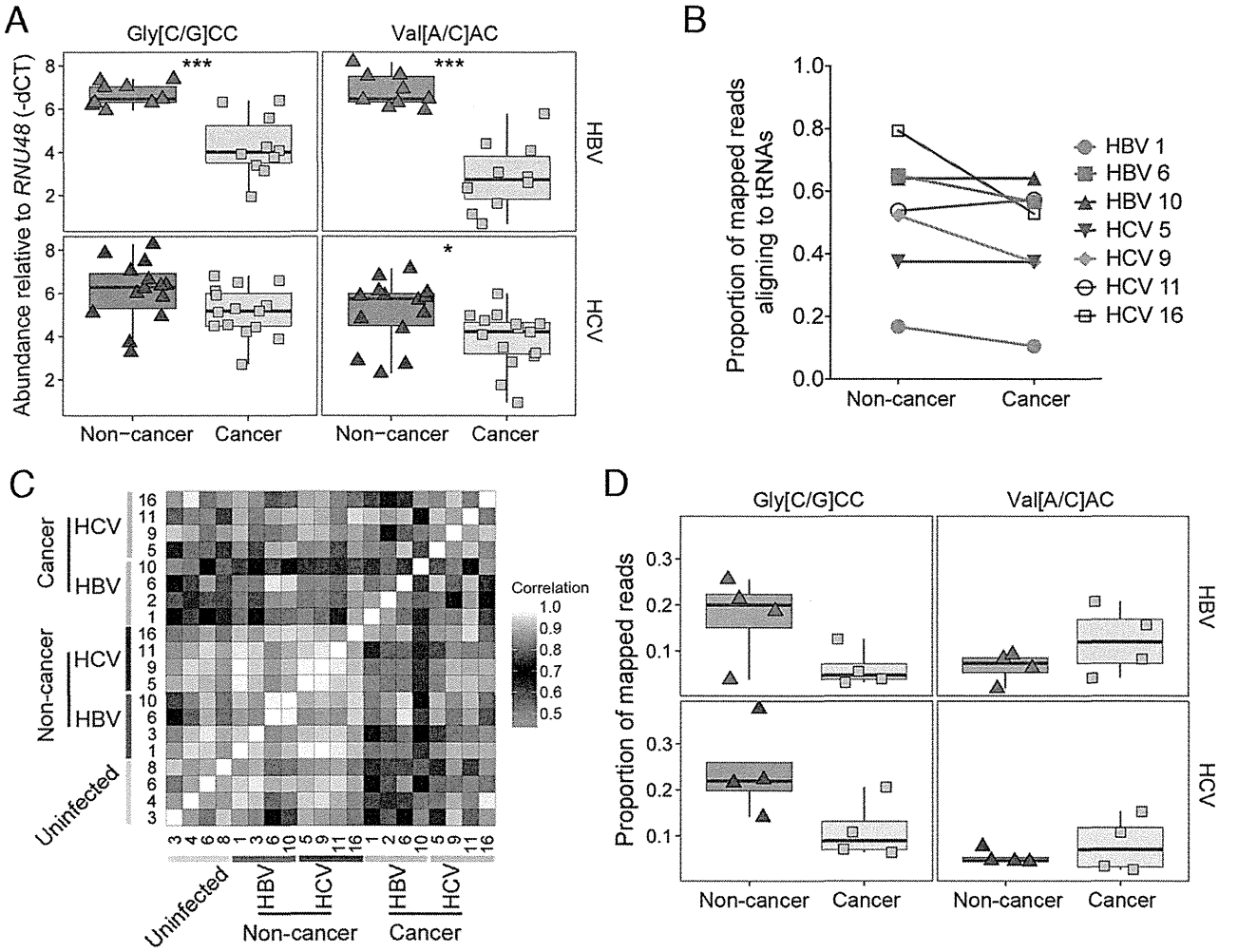

Figure 2 | 5′ tRH abundance in HBV- and HCV-associated hepatocellular carcinoma. (b) Abundance (RT-qPCR) of (left) 5′ tRH^{Gly} (Gly[C/G]CC) and (right) 5′ tRH^{Val} (Val[A/C]AC) in (top) non-malignant (n=9) and cancer tissue (n=10) from HBV-infected subjects, and (bottom) non-malignant (n=14), and cancer tissue (n=15) from HCV-infected subjects. Box and whisker plots are overlaid with data from each sample; whiskers extend to 1.5 * interquartile range. P-values calculated using Mann-Whitney U-test. *P < 0.05; **P < 0.01; ***P < 0.005. (b) Proportion of mapped reads aligning to tRNAs for the paired cancer and non-cancer tissue from subjects with chronic hepatitis B (n=3) and hepatitis C (n=4) (c) Correlation heatmap of tRNA-derived RNA expression profiles determined by small RNA sequencing. The colors of the cells represent Spearman's rank correlation coefficients of the relative levels of the 10 most abundant tRNA-derived RNAs between all pairs of tissue samples sequenced (n=20). (d) Proportion of mapped reads that align to 5′ tRH^{Gly} and 5′ tRH^{Val} in non-malignant and cancer tissue from (top) HBV-infected and (bottom) HCV-infected subjects. "Mapped reads" represents all reads aligning to miRNAs or tRNAs (see Methods).

abundance in seminal exosomes (considered to be immunosuppressive)[28], and roles in facilitating *Trypanosoma cruzi* infection in human cells and altering host gene expression[29].

There is good evidence that the abundance of these small non-coding RNAs increases in response to specific kinds of cellular stress. For example, tRHs are induced in cell culture by the addition of sodium arsenite, exposure to UV, nutrient starvation, hypoxia, hypothermia and heat, but not by exposure to etoposide, γ-radiation, caffeine[30,31]. This strongly suggests that the formation of tRHs is a regulated process, rather than due to general degradation of tRNAs in response to stress. In the nucleus angiogenin is involved in promoting angiogenesis[32] and in the cytoplasm, when not bound to RNH1, it acts as a tRNA-processing RNase[33,34], cleaving tRNAs at the anticodon loop and producing tRHs[30,31]. The cellular localization of angiogenin and its ribonuclease activity depend on the intracellular conditions and are regulated by RNH1[33]. The differences we observed in correlations between ANG expression and tRH abundance in chronic hepatitis B, hepatitis C and associated liver cancer may be a result of differences in angiogenin localization and function in these disease states. Non-tumor and tumor tissues from patients with chronic hepatitis C tend to show more evidence of angiogenesis than the in chronic hepatitis B[35,36]. This could mean that in chronic hepatitis C angiogenin is primarily nuclear, and therefore not exclusively involved in tRH production. Finally, it must also be noted that factors other than ANG may be critical to tRH biogenesis in different cell types or in response to different types of cellular stress. Much more remains to be uncovered about the specific mechanisms that lead to tRH accumulation.

Chronic infections with HBV and HCV typically lead to more severe liver disease in human patients than in the chimpanzee model[37,38]. Disease severity may account for the differences we observed in tRH abundance between liver tissue from human subjects with chronic HCV infection and the chimpanzee samples. Interestingly, however, humans and chimpanzees exhibited similar increases in tRH abundance in chronic hepatitis B, suggesting that

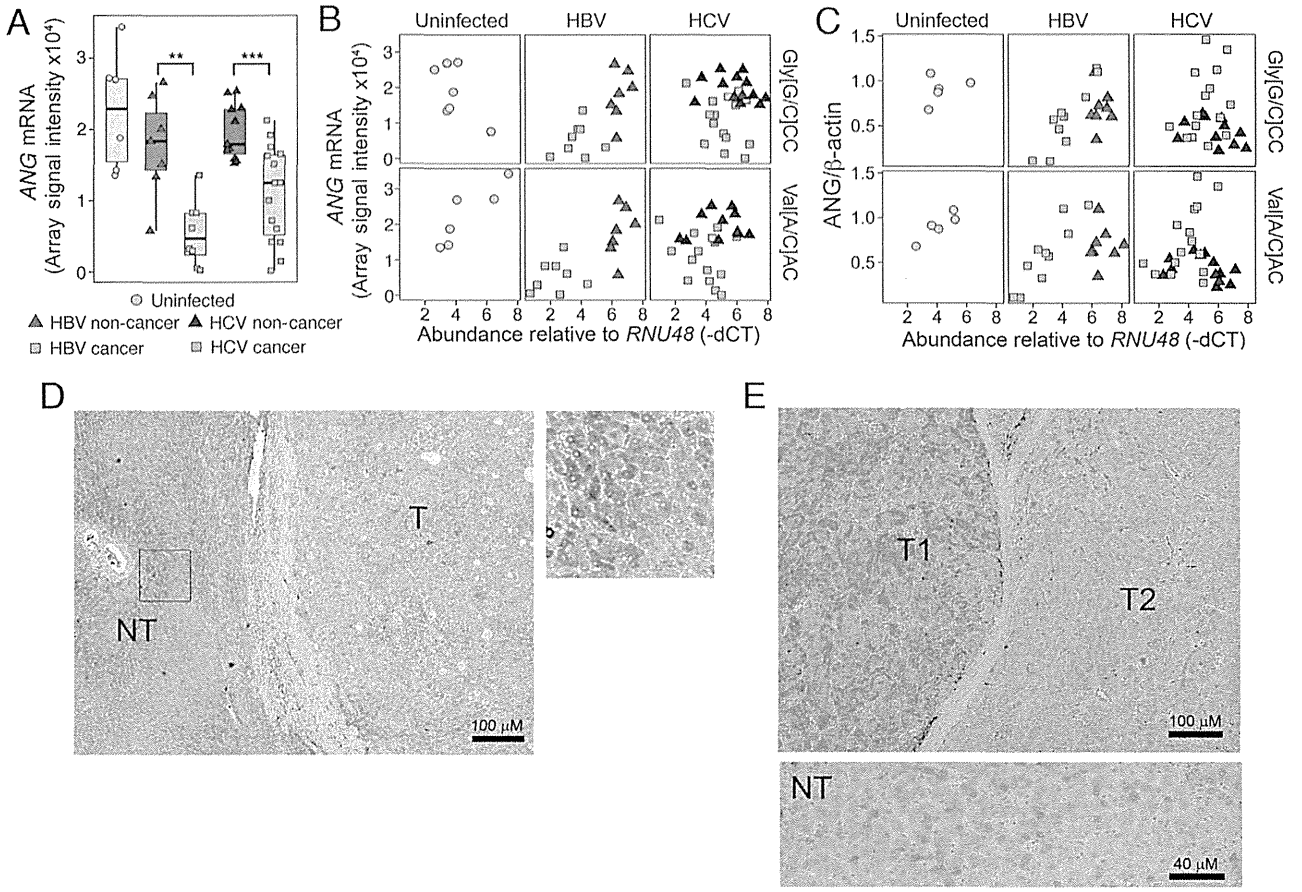

Figure 3 | Angiogenin expression in viral hepatitis and hepatocellular carcinoma. (a) Normalized *ANG* mRNA levels from previously generated liver microarray data[14] from uninfected subjects (n=6), non-malignant (n=7) and liver cancer (n=8) tissue from HBV-infected subjects, and non-malignant (n=11) and cancer tissue (n=15) from HCV-infected subjects. **P < 0.01; ***P < 0.005, calculated by Mann-Whitney *U*-test. (b) Scatter plot of the levels of 5′ tRHs (RT-qPCR, -dCT normalized to *RNU48*) and *ANG* mRNA (microarray). 5′ tRH^{Gly} ("Gly[C/G]CC"): uninfected subjects (n=7), non-cancer (n=7) and cancer (n=8) liver tissue from chronic hepatitis B subjects, and non-cancer (n=11) and cancer (n=15) liver tissue from chronic hepatitis C subjects; 5′ tRH^{Val}: uninfected subjects (n=6), non-cancer (n=7) and cancer (n=8) liver tissue from chronic hepatitis B subjects, and non-cancer (n=11) and cancer (n=15) liver tissue of chronic hepatitis C subjects. (c) Scatter plot of the levels of 5′ tRHs (RT-qPCR, -dCT normalized to *RNU48*) and ANG protein expression (normalized to β-actin) determined by immunoblot analysis. (d) Immunohistochemistry staining for ANG in formalin-fixed non-tumor (NT) and tumor tissue (T) from HBV-infected subject #10. (Right) Magnified view of non-tumor (NT). (e) ANG staining in adjacent tumor nodules (T1 and T2) and in non-tumor (NT) tissue from HCV-infected subject #7.

there may be a primary HBV-specific mechanism that directly regulates tRH biogenesis.

Our study has some technical limitations. tRNAs are subject to many different chemical modifications[39], several of which could impede library preparation and sequencing. This may have biased which tRNA-derived RNAs we detected. Also, we do not know how tRH abundance varies among the diverse cell types that populate the liver. Given that these small RNAs have not previously been studied in human tissue, we also have little appreciation of what functions these small non-coding RNAs have within the liver. Nonetheless, our finding that the intrahepatic abundance of tRHs is substantially increased in chronic viral infections of the liver and altered in HCC suggest that tRHs may have important, yet to be determined roles in liver disease. Thus, this study may have implications for disease pathogenesis and novel therapeutic strategies.

Methods

The methods were carried out in accordance with the approved guidelines.

Human subjects. Written informed consent was obtained from all human subjects. Ethics approval was obtained from the Ethics Committee for Human Genome/Gene Analysis Research at Kanazawa University Graduate School of Medical Science.

Chimpanzee liver tissue. The chimpanzee samples used in this study were archived from previous studies and were collected prior to December 15, 2011. Chimpanzees were housed and cared for at the Southwest National Primate Research Center (SNPRC) of the Texas Biomedical Research Institute. The animals were cared for in accordance with the Guide for the Care and Use of Laboratory Animals, and all protocols were approved by the Institutional Animal Care and Use Committee. SNPRC is accredited by the Association for Assessment and Accreditation of Laboratory Animal Care (AAALAC) International. SNPRC operates in accordance with the NIH and U.S. Department of Agriculture guidelines and the Animal Welfare Act. Animals were sedated for all procedures. Animals are group-housed with indoor and outdoor access and an environmental enrichment program is provided by a staff of behavioral scientists.

Small RNA-sequencing. RNA was isolated as described previously[14]. RNA purity was assessed with Nanodrop 2000 (Thermo Scientific) and integrity was determined with an Agilent 2100 Bioanalyzer (Agilent). RNA integrity and sequencing quality were comparable for all specimens (Supplemental Table 2–4). Small RNA libraries were generated using Illumina TruSeq Small RNA Sample Preparation Kit (Illumina, San Diego, CA). Sequencing was performed on Illumina HiSeq 2000 platform. Bioinformatic analysis: Sequencing reads were trimmed using Cutadapt (parameters O -10 e 0.1) and were further analyzed in two different ways: (i) Mapped trimmed reads allowing no mismatches to all tRNA sequences (except pseudo-tRNAs and undefined tRNAs) downloaded from GtRNAdb[16] (Figure 1b,c; Figure 2c,d; Supplemental Figure 1,2,4,7); (ii) Mapped trimmed reads to genomic regions spanning annotated miRNA s[40] (+/− 20 nts) and tRNA sequences (+/− 40 nts) using Bowtie 0.12.7[41] allowing for no mismatches. Next, reads that did not map

without mismatches were aligned to the same regions using SHRiMP2.2.2[42]. SHRiMP2.2.2 seeds were set based on the length of the read allowing 1 mismatch anywhere in the body and up to 3 mismatches at the 3′ end of the read (based on the length of the read). (Figure 1a right, Figure 2b, Supplemental Figure 7, Supplemental Table 4). Small RNA-sequencing data was deposited on GEO (GSE57381).

AGO2-RNA Co-immunoprecipitation. FT3-7 cells were grown in Dulbecco's modified Eagle's medium (DMEM, Life Technologies) and supplemented with 10% fetal calf serum and 2 mM GlutaMAX (Life Technologies, Carlsbad, CA). Cells were cultured in a humidified incubator at 37°C and 5% CO_2. Three technical replicates of 1×10^7 FT3-7 cells were harvested in lysis buffer [150 mM KCl, 25 mM Tris-HCl (pH 7.4), 5 mM EDTA, 1% Triton X-100, 5 mM DTT, Complete protease inhibitor mixture (Roche), and 100 U/mL RNaseOUT (Life Technologies)]. Lysates were centrifuged for 30 min at 17,000 × g at 4°C and filtered through a 0.22-um filter. Filtrates were incubated with anti-human AGO2 mAb (RN003M, MBL International, Woborn, MA) or isotype control IgG (Abcam, Cambridge, England) at 4°C for 2 h, followed by addition of 30 μL of Protein G Sepharose (GE Healthcare) for 1 h. The Sepaharose beads were washed three times in lysis buffer and RNA extracted using the miRNeasy Mini Kit (Qiagen, Hilden, Germany).

Small RNA real time quantitative PCR (RT-qPCR). Complementary DNA (cDNA) was synthesized using TaqMan MicroRNA Reverse Transcription Kit (Life Technologies) according to the manufacturer's instructions. Real time PCR amplification was performed using TaqMan Universal Master Mix (Life Technologies) on the Bio-Rad CFX96 real time PCR detection system. *U6*, miR-24, let-7a, let-7f, *RNU48*, and *RNU66* were all evaluated as potential housekeeping small RNAs for purposes of normalization. *RNU48* was selected because it was the most consistent across disease groups. RT-qPCR reactions for human samples were performed in triplicate. RT-qPCR reactions for chimpanzee samples were performed in duplicate. The following TaqMan assays were purchased from Life Technologies: miR-122 (product number 4427975; 002245) and *RNU48* or *SNORD48* (product number 4427975; 001006). Primers for the custom TaqMan assays (5′ tRH^{Gly} and 5′ tRH^{Val}) were designed using 5′-GCAUUGGUGGUUCAGUGGUAGAAU-UCUCGCCU-3′ for 5′ tRH^{Gly} and 5′-GUUUCCGUAGUGUAGUGGUUAUCAC-GUUCGCCU-3′ for 5′ tRH^{Val}.

Metabolic Radiolabeling and Measurement of Nascent Protein Synthesis. Huh7 cells were seeded onto the wells of 6-well cell culture plates at a density of 2×10^5 cells/well and incubated overnight to allow cell attachment. Cells were transfected with 50 nM and 100 nM of 5′ tRH^{Gly} (5′-GCAUUGGUGGUUCAGUGGUAGAAU-UCUCGCCU-3′), 5′ tRH^{Val} (5′-GUUUCCGUAGUGUAGUGGUUAUCACGUU-CGCCU-3′), or scramble (5′-GCAUUCACUUGGAUAGUAAAUCCAAGC-UGAA-3′)[21] (all from Integrated DNA Technologies, Coralville, IA) oligonucleotide after replacing cell culture medium with methionine- and cysteine-deficient DMEM (Life Technologies) and cultured for further 12 hrs. Cells were then metabolically radiolabeled for 12 hrs with 200 μCi/well of Express Protein Labeling Mix containing [^{35}S]methionine and [^{35}S]cysteine (PerkinElmer, Waltham, MA) in the presence or absence of 50 μg/ml puromycin and lysed with lysis buffer (20 mM Tris-HCl [pH 7.4] containing 150 mM NaCl, 1% Triton X-100, 0.05% SDS, and 10% glycerol) supplemented with 50 mM NaF, 5 mM Na_3VO_4, and a protease inhibitor cocktail (Complete; Roche, Mannheim, Germany). The protein concentration of cell lysates was determined by the Bio-Rad Protein Assay (Bio-Rad), and 10 μg (total protein) of cell lysates was subjected to SDS-PAGE followed by staining gels with the Sypro Ruby Protein Gel Stain (Bio-Rad, Hercules, CA) and autoradiography.

Immunohistochemistry (IHC). Staining was performed by immunoperoxidase technique with an Envision kit (DAKO Japan). Primary antibodies used were against β-actin (Cell signaling technology, #4967, Beverly, MA) and Human Angiogenin Affinity Purified Polyclonal Ab (R and D Systems, AF265, Minneapolis, MN).

1. Arzumanyan, A., Reis, H. M. & Feitelson, M. A. Pathogenic mechanisms in HBV- and HCV-associated hepatocellular carcinoma. *Nat Rev Cancer* **13**, 123–135 (2013).
2. Perz, J. F., Armstrong, G. L., Farrington, L. A., Hutin, Y. J. & Bell, B. P. The contributions of hepatitis B virus and hepatitis C virus infections to cirrhosis and primary liver cancer worldwide. *J Hepatol* **45**, 529–538 (2006).
3. Hou, W. & Bonkovsky, H. L. Non-coding RNAs in hepatitis C-induced hepatocellular carcinoma: dysregulation and implications for early detection, diagnosis and therapy. *World J Gastroenterol* **19**, 7836–7845 (2013).
4. Xu, X. *et al.* Hepatitis B virus X protein represses miRNA-148a to enhance tumorigenesis. *J Clin Invest* **123**, 630–645 (2013).
5. Chen, Y. *et al.* HCV-induced miR-21 contributes to evasion of host immune system by targeting MyD88 and IRAK1. *PLoS Pathog* **9**, e1003248 (2013).
6. Jopling, C. L., Yi, M., Lancaster, A. M., Lemon, S. M. & Sarnow, P. Modulation of hepatitis C virus RNA abundance by a liver-specific MicroRNA. *Science* **309**, 1577–1581 (2005).
7. Shimakami, T. *et al.* Stabilization of hepatitis C virus RNA by an Ago2-miR-122 complex. *Proc Natl Acad Sci U S A* **109**, 941–946 (2012).
8. Janssen, H. L. *et al.* Treatment of HCV Infection by Targeting MicroRNA. *N Engl J Med* **368**, 1685–1694 (2013).
9. Garcia-Silva, M. R., Cabrera-Cabrera, F. & Güida, M. C. Hints of tRNA-Derived Small RNAs Role in RNA Silencing Mechanisms. *Genes* **3**, 603–614 (2012).
10. Wang, Q. *et al.* Identification and functional characterization of tRNA-derived RNA fragments (tRFs) in respiratory syncytial virus infection. *Mol Ther* **21**, 368–379 (2013).
11. Gong, B. *et al.* Compartmentalized, functional role of angiogenin during spotted fever group rickettsia-induced endothelial barrier dysfunction: evidence of possible mediation by host tRNA-derived small noncoding RNAs. *BMC Infect Dis* **13**, 285 (2013).
12. Saikia, M. *et al.* Angiogenin-Cleaved tRNA Halves Interact with Cytochrome c Protecting Cells from Apoptosis during Osmotic Stress. *Mol Cell Biol* **34**, 2450–63 (2014).
13. Hou, J. *et al.* Identification of miRNomes in human liver and hepatocellular carcinoma reveals miR-199a/b-3p as therapeutic target for hepatocellular carcinoma. *Cancer Cell* **2**, 232–243 (2011).
14. Spaniel, C., Honda, M., Selitsky, S. R. & Yamane, D. microRNA-122 abundance in hepatocellular carcinoma and non-tumor liver tissue from Japanese patients with persistent HCV versus HBV infection. *PloS One* **8**, e76867 (2013).
15. Bartel, D. P. MicroRNAs: target recognition and regulatory functions. *Cell* **136**, 215–233 (2009).
16. Chan, P. P. & Lowe, T. M. GtRNAdb: a database of transfer RNA genes detected in genomic sequence. *Nucleic Acids Res* **37**, D93–97 (2009).
17. Kozomara, A. & Griffiths-Jones, S. miRBase: annotating high confidence microRNAs using deep sequencing data. *Nucleic Acids Res* **42**, D68–73 (2014).
18. Lanford, R. E., Lemon, S. M. & Walker, C. in *Hepatitis C Antiviral Drug Discovery & Development* (eds He, Y. & Tan, T.) 99–132 (Horizons Scientific Press, 2011).
19. Asabe, S. *et al.* The size of the viral inoculum contributes to the outcome of hepatitis B virus infection. *J Virol* **83**, 9652–9662 (2009).
20. Fu, H. *et al.* Stress induces tRNA cleavage by angiogenin in mammalian cells. *FEBS Lett* **583**, 437–442 (2009).
21. Yamasaki, S., Ivanov, P., Hu, G.-F. & Anderson, P. Angiogenin cleaves tRNA and promotes stress-induced translational repression. *J Cell Biol* **185**, 35–42 (2009).
22. Wang, Q. *et al.* Identification and functional characterization of tRNA-derived RNA fragments (tRFs) in respiratory syncytial virus infection. *Mol Ther* **21**, 368–379 (2013).
23. Gong, B. *et al.* Compartmentalized, functional role of angiogenin during spotted fever group rickettsia-induced endothelial barrier dysfunction: evidence of possible mediation by host tRNA-derived small noncoding RNAs. *BMC Infect Dis* **13**, 285 (2013).
24. Mishima, E. *et al.* Conformational Change in Transfer RNA Is an Early Indicator of Acute Cellular Damage. *J Am Soc Nephrol* **25**, 2316–26 (2014).
25. Ivanov, P., Emara, M. M., Villen, J., Gygi, S. P. & Anderson, P. Angiogenin-induced tRNA fragments inhibit translation initiation. *Mol Cell* **43**, 613–623 (2011).
26. Emara, M. M. *et al.* Angiogenin-induced tRNA-derived stress-induced RNAs promote stress-induced stress granule assembly. *J Biol Chem* **285**, 10959–10968 (2010).
27. Dhahbi, J. M. *et al.* 5′ tRNA halves are present as abundant complexes in serum, concentrated in blood cells, and modulated by aging and calorie restriction. *BMC Genomics* **14**, 298 (2013).
28. Vojtech, L. *et al.* Exosomes in human semen carry a distinctive repertoire of small non-coding RNAs with potential regulatory functions. *Nucleic Acids Res* **42**, 7290–7304 (2014).
29. Garcia-Silva, M. R. *et al.* Gene Expression Changes Induced by Trypanosoma cruzi Shed Microvesicles in Mammalian Host Cells: Relevance of tRNA-Derived Halves. *Biomed Res Int* **2014**, 305239 (2014).
30. Fu, H. *et al.* Stress induces tRNA cleavage by angiogenin in mammalian cells. *FEBS Lett* **583**, 437–442 (2009).
31. Yamasaki, S., Ivanov, P., Hu, G.-F. & Anderson, P. Angiogenin cleaves tRNA and promotes stress-induced translational repression. *J Biol Chem* **185**, 35–42 (2009).
32. Gao, X. & Xu, Z. Mechanisms of action of angiogenin. *Acta Biochim Biophys Sin (Shanghai)* **40**, 619–624 (2008).
33. Pizzo, E. *et al.* Ribonuclease/angiogenin inhibitor 1 regulates stress-induced subcellular localization of angiogenin to control growth and survival. *J Cell Sci* **126**, 4308–4319 (2013).
34. Saxena, S. K., Rybak, S. M., Davey, R. T., Youle, R. J. & Ackerman, E. J. Angiogenin is a cytotoxic, tRNA-specific ribonuclease in the RNase A superfamily. *J Biol Chem* **267**, 21982–21986 (1992).
35. Mazzanti, R. *et al.* Chronic viral hepatitis induced by hepatitis C but not hepatitis B virus infection correlates with increased liver angiogenesis. *Hepatology* **25**, 229–234 (1997).
36. Messerini, L., Novelli, L. & Comin, C. E. Microvessel density and clinicopathological characteristics in hepatitis C virus and hepatitis B virus related hepatocellular carcinoma. *J Clin Pathol* **57**, 867–871 (2004).
37. Walker, C. M. Comparative features of hepatitis C virus infection in humans and chimpanzees. *Springer Semin Immunopathol* **19**, 85–98 (1997).
38. Mason, W. S. *et al.* Detection of clonally expanded hepatocytes in chimpanzees with chronic hepatitis B virus infection. *J Virol* **83**, 8396–8408 (2009).
39. Jackman, J. E. & Alfonzo, J. D. Transfer RNA modifications: nature's combinatorial chemistry playground. *Wiley Interdisciplin Rev RNA* **4**, 35–48 (2013).

40. Kozomara, A. & Griffiths-Jones, S. miRBase: annotating high confidence microRNAs using deep sequencing data. *Nucleic Acids Res* **42**, D68–73 (2014).
41. Langmead, B., Trapnell, C., Pop, M. & Salzberg, S. L. Ultrafast and memory-efficient alignment of short DNA sequences to the human genome. *Genome Biol* **10**, R25 (2009).
42. David, M., Dzamba, M., Lister, D., Ilie, L. & Brudno, M. SHRiMP2: sensitive yet practical short read mapping. *Bioinformatics* **27**, 1011–2 (2011).
43. Larkin, M. A., Blackshields, G., Brown, N. P. & Chenna, R. Clustal W and Clustal X version 2.0. *Bioinformatics* **23**, 2947–2948 (2007).

Acknowledgments

This work was supported by grants from the National Institutes of Health: R00-DK091318 (P.S.); R01-AI095690 and R01-CA164029 (S.M.L); T32-GM067553 and T32-AI007419 (S.R.S). The Southwest National Primate Research Center is supported by a grant from the NIH Office of Research Infrastructure Programs/OD P51 OD011133), and by Research Facilities Improvement Program Grants C06 RR 12087 and C06 RR016228.

Author contributions

The experiments were designed by S.R.S., P.S. and S.M.L. The data were analyzed by S.R.S., J.B., T. Shirasaki, M.H., P.S. and S.M.L. Experiments were performed by S.R.S., D.Y., T.M., E.E.F., B.G. and T. Shirasaki. M.H., T. Shimakami, S.K., R.E.L., S.M.L. and P.S. contributed resources. The manuscript was written by S.R.S., P.S. and S.M.L.

Additional information

Supplementary information accompanies this paper at http://www.nature.com/scientificreports

Competing financial interests: The authors declare no competing financial interests.

How to cite this article: Selitsky, S.R. *et al.* Small tRNA-derived RNAs are increased and more abundant than microRNAs in chronic hepatitis B and C. *Sci. Rep.* **5**, 7675; DOI:10.1038/srep07675 (2015).

HEPATOLOGY
Official Journal of the American Association for the Study of Liver Diseases

Impaired Interferon Signaling in Chronic Hepatitis C Patients With Advanced Fibrosis via the Transforming Growth Factor Beta Signaling Pathway

Takayoshi Shirasaki,[1,2] Masao Honda,[1,2] Tetsuro Shimakami,[1] Kazuhisa Murai,[1,2] Takayuki Shiomoto,[1,2] Hikari Okada,[1] Riuta Takabatake,[1] Akihiro Tokumaru,[1] Yoshio Sakai,[1] Taro Yamashita,[1] Stanley M. Lemon,[3] Seishi Murakami,[1] and Shuichi Kaneko[1]

Malnutrition in the advanced fibrosis stage of chronic hepatitis C (CH-C) impairs interferon (IFN) signaling by inhibiting mammalian target of rapamycin complex 1 (mTORC1) signaling. However, the effect of profibrotic signaling on IFN signaling is not known. Here, the effect of transforming growth factor (TGF)-β signaling on IFN signaling and hepatitis C virus (HCV) replication was examined in Huh-7.5 cells by evaluating the expression of forkhead box O3A (Foxo3a), suppressor of cytokine signaling 3 (Socs3), c-Jun, activating transcription factor 2, ras homolog enriched in brain, and mTORC1. The findings were confirmed in liver tissue samples obtained from 91 patients who received pegylated-IFN and ribavirin combination therapy. TGF-β signaling was significantly up-regulated in the advanced fibrosis stage of CH-C. A significant positive correlation was observed between the expression of TGF-β2 and mothers against decapentaplegic homolog 2 (Smad2), Smad2 and Foxo3a, and Foxo3a and Socs3 in the liver of CH-C patients. In Huh-7.5 cells, TGF-β1 activated the Foxo3a promoter through an AP1 binding site; the transcription factor c-Jun was involved in this activation. Foxo3a activated the Socs3 promoter and increased HCV replication. TGF-β1 also inhibited mTORC1 and IFN signaling. Interestingly, c-Jun and TGF-β signaling was up-regulated in treatment-resistant IL28B minor genotype patients (TG/GG at rs8099917), especially in the early fibrosis stage. Branched chain amino acids or a TGF-β receptor inhibitor canceled these effects and showed an additive effect on the anti-HCV activity of direct-acting antiviral drugs (DAAs). *Conclusion:* Blocking TGF-β signaling could potentiate the antiviral efficacy of IFN- and/ or DAA-based treatment regimens and would be useful for the treatment of difficult-to-cure CH-C patients. (HEPATOLOGY 2014;60:1519-1530)

A human liver infected with hepatitis C virus (HCV) develops chronic hepatitis, cirrhosis, and in some instances, hepatocellular carcinoma (HCC). HCC develops frequently in the advanced fibrosis stage, and the annual incidence of HCC in patients with HCV-related liver cirrhosis is ~6-8%.[1] The eradication of HCV infection has been a promising prophylactic therapy for preventing the occurrence of HCC.

Interferon (IFN) and ribavirin (RBV) combination therapy has been a popular modality for eliminating HCV; however, its efficacy is limited in patients with advanced liver fibrosis.[2] The use of the recently developed direct-acting antiviral drugs (DAAs) telaprevir or

Abbreviations: AMPK, protein kinase, AMP-activated, alpha 1 catalytic subunit; CH-C, chronic hepatitis C; HCC, hepatocellular carcinoma; HCV, hepatitis C virus; IFN, interferon; IL28B, interleukin 28B; ISG-20, interferon-stimulated exonuclease gene 20; MX1, myxovirus resistance 1; NR, no response; RBV, ribavirin; RHEB, ras homolog enriched in brain; RIG-I, retinoic acid inducible gene I; SMAD, mothers against decapentaplegic homolog; TGF, transforming growth factor; TGF-RI, transforming growth factor-receptor inhibitor.

From the [1]Department of Gastroenterology, Kanazawa University Graduate School of Medicine, Kanazawa, Japan; [2]Department of Advanced Medical Technology, Kanazawa University Graduate School of Health Medicine, Kanazawa, Japan; [3]Division of Infectious Diseases, School of Medicine, University of North Carolina at Chapel Hill, Chapel Hill, NC, USA.

Received February 1, 2014; accepted June 20, 2014.

boceprevir, combined with pegylated (PEG)-IFN plus RBV, significantly improved the sustained virologic response (SVR) rates; however, the SVR rate is reduced in patients with advanced liver fibrosis and the treatment-resistant interleukin 28B (IL28B) genotype,[3-5] in whom HCC can develop at a high frequency. Moreover, extended therapy should be avoided in these patients in terms of the high frequency of adverse effects.

The mechanism of treatment resistance in patients with advanced liver fibrosis has not yet been clarified completely. Previously, we reported that the malnutrition status of patients with advanced chronic hepatitis C (CH-C) is associated with IFN resistance, and Fischer's ratio (branched chain amino acids [BCAAs] / aromatic amino acids) is an independent predictor of treatment outcome of PEG-IFN plus RBV combination therapy. Furthermore, we showed that malnutrition impaired IFN signaling by inhibiting mammalian target of rapamycin complex 1 (mTORC1) and activating suppressor of cytokine signaling 3 (Socs3)-mediated IFN inhibitory signaling through the nutrition-sensing transcriptional factor forkhead box protein O3a (Foxo3a).[6] This report represented the first clue to disentangling the molecular links between advanced CH-C and poor treatment response; however, the association of profibrotic signaling and IFN signaling was not evaluated in detail.

In the present study, we investigated the interaction between the signaling of the profibrotic gene transforming growth factor (TGF)-β and IFN signaling in the liver of CH-C patients. We showed that blocking TGF-β signaling as well as improving the nutritional status of patients by using BCAAs restored IFN signaling and increased the treatment efficacy of anti-HCV therapy.

Materials and Methods

Cell Lines. A reversibly immortalized human hepatocyte cell line (TTNT) was established by transduction with a retroviral vector containing cDNA expressing hTERT for immortalization.[7] TTNT, Huh-7, and Huh-7.5 cells (kindly provided by Professor C.M. Rice, Rockefeller University, New York, NY) were maintained in Dulbecco's modified Eagle's medium (DMEM; Gibco BRL, Gaithersburg, MD) containing 10% fetal bovine serum and 1% penicillin/streptomycin. Primary human hepatocytes (PHH) were isolated from chimeric mice with a humanized liver (PXB-mice; PhoenixBio, Hiroshima, Japan).

Amino Acid-Free Medium and BCAAs. Amino acid-free medium and BCAAs were prepared as described previously. Details are given in the Supporting Materials and Methods.

TGF-β and IFN Treatment. Huh-7.5 cells or HCV-RNA-transfected Huh-7.5 cells were seeded at 1.0×10^5 cells/well in 12-well plates. After 24 hours, the cells were treated with TGF-β (Millipore, Billerica, MA). At 24 hours later, the cells were treated with the indicated international units of IFN-α for 24 hours (Schering-Plough, Tokyo, Japan).

BCAA Treatment. HCV-RNA-transfected Huh-7.5 cells were seeded at 1.0×10^5 cells/well in 12-well plates. After 24 hours, the cells were treated with TGF-β in low-amino-acid medium and the indicated concentration of BCAAs. At 48 hours after treatment, real-time detection, polymerase chain reaction (RTD-PCR), western blotting, and *Gaussia* luciferase assays were carried out as described previously.

TGF-β Receptor Inhibitor Treatment. HCV-RNA-transfected Huh-7.5 cells were seeded at 1.0×10^5 cells/well in 12-well plates. After 24 hours, the cells were treated with TGF-β in low-amino-acid medium and TGF-β Receptor Inhibitor (TGF-β RI; Millipore). At 24 hours after treatment, RTD-PCR, western blotting, and *Gaussia* luciferase assays were carried out as described previously.

DAA Treatment. DAAs (boceprevir and BMS-790052) were purchased from AdooQ Bioscience (Irvine, CA). HCV-RNA-transfected Huh-7.5 cells were seeded at 1.0×10^5 cells/well in 12-well plates. After 24 hours, the cells were treated with TGF-β in low-amino-acid medium and BCAAs and DAAs. At 24 hours after treatment, the *Gaussia* luciferase assay was carried out as described previously.

Patients' characteristics, HCV replication analysis, western blotting, quantitative RTD-PCR, and promoter analysis are described in the Supporting Materials and Methods.

Address reprint requests to: Masao Honda, M.D., Ph.D., Department of Gastroenterology, Graduate School of Medicine, Kanazawa University, Takara-Machi 13-1, Kanazawa 920-8641, Japan. E-mail: mhonda@m-kanazawa.jp; fax: +81-76-234-4250.

View this article online at wileyonlinelibrary.com.

DOI 10.1002/hep.27277

Potential conflict of interest: Nothing to report.

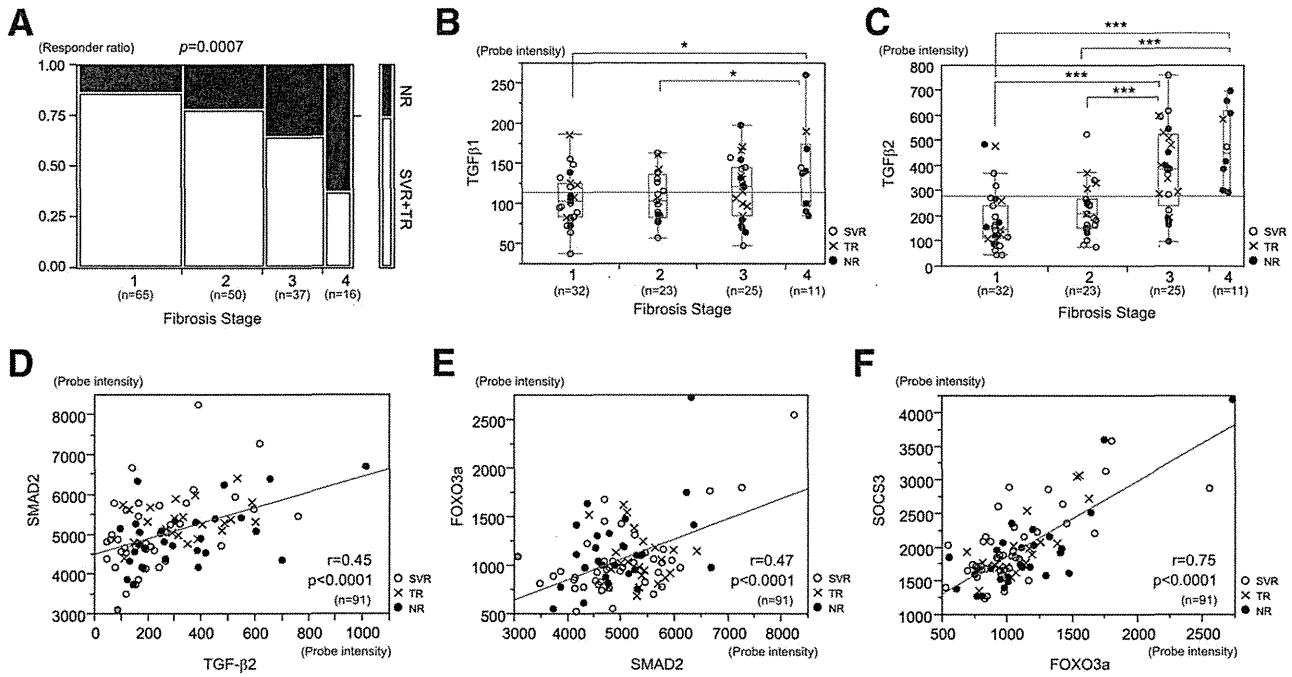

Fig. 1. Activation of TGF-β signaling in the liver of patients at the advanced fibrosis stage of CH-C. A: Significant increase in the NR ratio with the progression of fibrosis stage. B,C: Expression of TGF-β1 (B) and TGF-β2 (C) with the progression of fibrosis stage. D-F: Significant correlations of TGF-β2 and Smad2 (D), Smad2 and Foxo3a (E), and Foxo3a and Socs3 (F) expression in the liver of CH-C patients.

Statistical Analysis. The results are expressed as the mean value ± standard deviation. At least three samples were tested in each assay. Significance was tested by one-way analysis of variance with Bonferroni methods, and differences were considered statistically significant at $P < 0.05$.

Results

Up-Regulated TGF-β Signaling and Low Treatment Response in CH-C Patients With Advanced Liver Fibrosis Who Received PEG-IFN Plus RBV Combination Therapy. Previously, using a cohort of 168 CH-C patients who received PEG-IFN plus RBV combination therapy, we demonstrated that liver fibrosis stage and Fischer's ratio as well as IL28B genotype were independent significant factors associated with no response (NR) to treatment (Supporting Table 1).[6] The NR rate was significantly increased according to the increase in fibrosis stage ($P = 0.007$) (Fig. 1A). To reveal the molecular mechanism between profibrotic signaling and treatment resistance, we focused on TGF-β signaling in the liver of CH-C patients. The expression of TGF-β1 and TGF-β2, deduced from 91 CH-C patients whose liver tissues were analyzed previously using an Affymetrix GeneChip (Supporting Table 2),[6,8] was significantly up-regulated in the advanced fibrosis stage (Fig. 1B,C). In particular, the up-regulation of TGF-β2 in patients with stage 3 and 4 fibrotic livers was more prominent (Fig. 1C). There was a significant correlation between the expression of TGF-β2 and mothers against decapentaplegic homolog 2 (Smad2), a downstream signaling molecule of the TGF-β receptor, showing the activation of TGF-β signaling in the liver of CH-C patients. Interestingly, Smad2 expression was significantly correlated with Foxo3a expression, a nutrition-sensing transcription factor. Previously, we reported that Foxo3a increases the transcription of Socs3, an inhibitor of IFN signaling, through binding to the Socs3 promoter (Foxo3a-Socs3 signaling).[6] Foxo3a expression was significantly correlated with Socs3 expression in the CH-C patients (Fig. 1F).

TGF-β Signaling Activates Foxo3a-Socs3 Signaling in the Huh-7.5 Human Hepatoma Cell Line and PHH. The relationship between TGF-β and Foxo3a-Socs3 signaling was evaluated in PHH and the Huh-7.5 human hepatoma cell line without HCV replication (Huh-7.5 HCV (–)). This signaling was also evaluated in Huh-7.5 cells in which the infectious HCV clone H77Sv3 GLuc2A[6] was replicating (Huh-7.5 HCV (+)) (Fig. 2A). Treatment of these cells with TGF-β1 substantially increased the levels of phosphorylated (p)-Smad2 and p-Smad3. In this condition, the levels of p-Foxo3a, which is degraded through the proteasomal pathway,

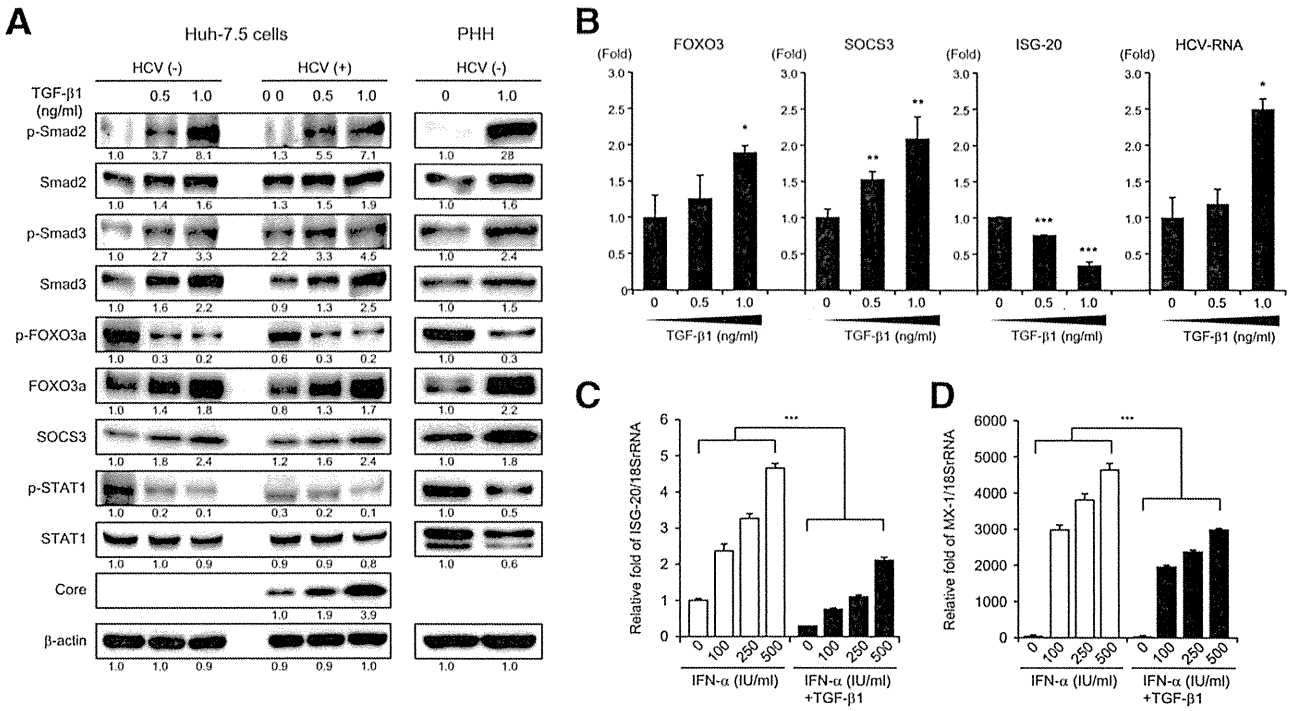

Fig. 2. Effect of TGF-β1 on IFN signaling in Huh-7.5 cells and PHH. A: Western blotting of TGF-β, Foxo3a-Socs3, and IFN signaling in Huh-7.5 cells and PHH treated with TGF-β1. Huh-7.5 cells were transfected with infectious HCV RNA, H77Sv3 GLuc2A prior to TGF-β1 treatment (Huh-7.5 HCV (+)). The experiments were repeated 3 times. B: RTD-PCR results for Foxo3a, Socs3, ISG-20, and HCV-RNA expression in Huh-7.5 HCV (+) treated with TGF-β1. C,D: Inhibition of IFN-α-induced ISG induction (ISG-20 [C] and MX1 [D]) by TGF-β1 in Huh-7.5 HCV (+). B-D: The experiments were performed in triplicate and repeated 3 times ($*P < 0.05$, $**P < 0.01$, $***P < 0.001$).

decreased and total Foxo3a expression increased, and then Socs3 expression increased. Subsequently, the levels of phosphorylated signal transducer and activator of transcription 1 (p-STAT1) were decreased and the amount of HCV core protein increased in Huh-7.5 HCV (+). Thus, TGF-β signaling activated Foxo3a-Socs3 signaling and inhibited IFN signaling in hepatocytes, regardless of HCV replication and a loss-of-function mutation in retinoic acid inducible gene I (RIG-I).

These findings were also confirmed at the mRNA level in Huh-7.5 HCV (+). RTD-PCR showed that TGF-β1 treatment significantly increased Foxo3a and Socs3 expression, and decreased the expression of interferon-stimulated exonuclease gene 20 (ISG-20) in a dose-dependent manner. HCV-RNA was significantly increased in this condition (Fig. 2B). Moreover, the induction of interferon-stimulated genes (ISG-20 and myxovirus-resistance 1 [MX1]) by IFN-α treatment was significantly reduced in the presence of TGF-β1 (Fig. 2C,D).

When endogenous TGF-β signaling was compared between Huh-7.5 HCV (–) and Huh-7.5 HCV (+), TGF-β signaling was preactivated in Huh-7.5 HCV (+) before TGF-β1 treatment (Fig. 2A). To examine the role of endogenous TGF-β1 signaling on Foxo3a-Socs3 signaling and HCV replication, a small interfering (si) RNA specific to TGF-β1 was introduced to Huh-7 cells in which cell culture-derived infectious HCV HJ3-5 (HCVcc HJ3-5)[9] (Supporting Materials and Methods) was replicating. With the repression of TGF-β1, the levels of p-Smad2, p-Smad3, Foxo3a, and Socs3a decreased, while the levels of p-STAT1 increased. As a result, HCV replication deceased in both the amino acid-depleted (1/5 DMEM) and non-depleted (DMEM) conditions (Supporting Fig. 1).

AP1 Binding Site in the Foxo3a Promoter Is Responsible for the Induction of Foxo3a by TGF-β Signaling. To identify which transcription factors were involved in the induction of Foxo3a by TGF-β1, we cloned the upstream promoter region of Foxo3a and generated Foxo3a promoter-luciferase reporter constructs with various lengths of 5′-end deletions (−1780, −1340, and −801 nucleotides [nt]) (Fig. 3A). Luciferase activity deduced from pGL4-FOXO3a (−1780) increased by ~1.5-fold in the amino acid-depleted condition (1/5 DMEM) compared with the nondepleted condition (DMEM). TGF-β1 further stimulated the promoter activity of pGL4-FOXO3a (−1780) (Fig. 3B). A TGF-β1 RI canceled this stimulation (Fig. 3B). pGL4-FOXO3a (−1340) retained the regulation of promoter activity by amino acid depletion (1/5 DMEM) and

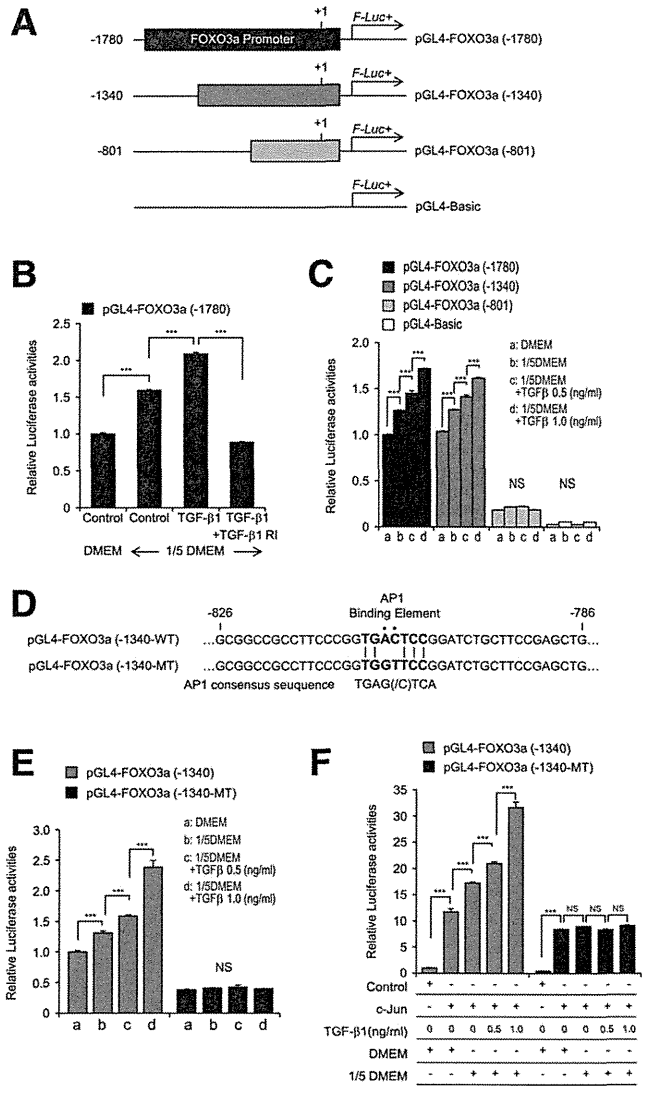

Fig. 3. Foxo3a promoter analysis. A: Foxo3a promoter-luciferase reporter constructs. B: Promoter activity of pGL4-FOXO3a (−1780) following amino acid depletion (1/5 DMEM), TGF-β1 treatment, and TGF-β1 RI treatment. C: Abolished regulation of the promoter activity of pGL4-FOXO3a (−801) by amino acid depletion (1/5 DMEM) and TGF-β1 treatment. D: Alignment of the AP1 binding element of pGL4-FOXO3a (−1340) and pGL4-FOXO3a (−1340-MT), in which the AP1 site was mutated. E: Abolished regulation of the promoter activity of pGL4-FOXO3a (−1340-MT) by amino acid depletion (1/5 DMEM) and TGF-β1 treatment. F: Overexpression of c-Jun, amino acid depletion (1/5 DMEM), and TGF-β1 treatment increased the promoter activity of pGL4-FOXO3a (−1340) by up to 32-fold, while these had less of an effect on the promoter activity of pGL4-FOXO3a (−1340-MT). The experiments were performed in triplicate and repeated 3 times (*$P < 0.05$, **$P < 0.01$, ***$P < 0.001$).

TGF-β1 treatment; however, pGL4-FOXO3a (−801) lost this regulation (Fig. 3C), suggesting the presence of a response element between −1340 and −801 nt. We identified an activator protein (AP) 1 transcription factor binding site at −810 to −804 nt. (Fig. 3D). We introduced two nucleotide mutations (AC to GT) in the AP1 consensus binding sequence, and the mutant construct, pGL4-FOXO3a (−1340-MT), lost the response to amino acid depletion (1/5 DMEM) and TGF-β1 treatment (Fig. 3E). These results were confirmed by using three different hepatocyte-derived cell lines (TTNT, Huh-7, and Huh-7.5 cells; Supporting Fig. 2A-C). Although RIG-I-dependent IFN signaling was active in TTNT cells (Supporting Fig. 2D), Foxo3a promoter activity in response to amino acid depletion (1/5 DMEM) and TGF-β1 treatment was not significantly different between these cell lines.

To confirm these findings further, we overexpressed c-Jun, a component of AP1, and evaluated Foxo3a promoter activity. The overexpression of c-Jun increased the promoter activity of pGL4-FOXO3a (−1340) to 12-fold, and amino acid depletion (1/5 DMEM) and TGF-β1 treatment further increased promoter activity up to 32-fold (Fig. 3F). Conversely, pGL4-FOXO3a (−1340-MT) lost the response to amino acid depletion (1/5 DMEM) and TGF-β1 treatment (Fig. 3F). These results confirmed that AP1 plays an important role in the induction of Foxo3a by these stimulatory factors.

Transcription Factor c-Jun Is Involved in the Induction of Foxo3a in the Liver of CH-C Patients. The AP1 transcription factor is mainly composed of Jun, Fos, and activating transcription factor (ATF) protein dimers.[10] Therefore, we evaluated the expression of c-Jun, ATF2, and c-Fos in Huh-7.5 cells and PHH under amino acid depletion (1/5 DMEM) and TGF-β1 treatment. Western blotting analysis showed that the levels of p-c-Jun and p-ATF2 were increased under these conditions, although the induction of p-c-Jun by amino acid depletion (1/5 DMEM) was not obvious in PHH (Fig. 4A). These findings were also confirmed by RTD-PCR. The mRNA expression of c-Jun and ATF2 increased significantly, while the expression of c-Fos decreased (Supporting Fig. 3A-C). The overexpression of c-Jun in Huh-7.5 cells induced Foxo3a and Socs3 expression at the protein and mRNA levels (Supporting Fig. 3D,E). In the liver of CH-C patients, there were significant correlations between the expression of Smad2 and c-Jun, and c-Jun and Foxo3a (Fig. 4B,C). ATF2 expression was significantly correlated with c-Jun expression (Fig. 4D). Similarly, there were significant correlations between the expression of Smad2 and ATF2, and ATF2 and Foxo3a (Fig. 4E,F). These results suggested that c-Jun and possibly ATF2, but not c-Fos, might be involved in TGF-β-Foxo3a signaling.

TGF-β Signaling Induces Socs3 Through the Induction of Foxo3a. Previously, we reported that Foxo3a increases the transcription of Socs3 through its binding to the Socs3 promoter region.[6] We confirmed

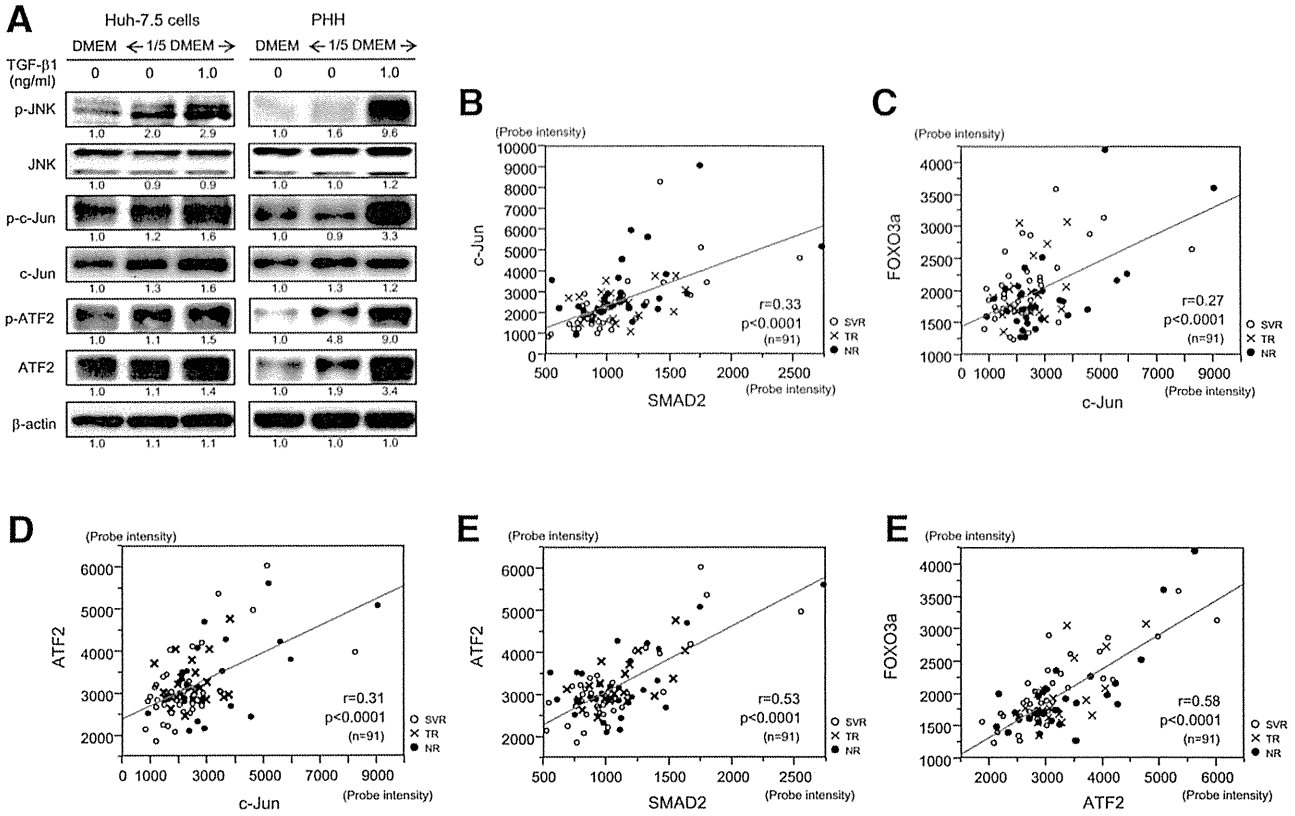

Fig. 4. TGF-β signaling up-regulates the expression of the transcription factors c-Jun and ATF2 in Huh-7.5 cells, PHH, and the liver of CH-C patients. A: Western blotting of JNK, c-Jun, and ATF2 in Huh-7.5 cells and PHH treated with amino acid depletion (1/5 DMEM) and TGF-β1. The experiments were repeated 3 times. B-F: Significant correlations of Smad2 and c-Jun (B), Foxo3a and c-Jun (C), c-Jun and ATF2 (D), Smad2 and ATF2 (E), and ATF2 and Foxo3a (F) expression in the liver of CH-C patients.

these findings in more detail in conjunction with TGF-β signaling. The overexpression of Foxo3a increased Socs3 expression in the nonamino acid-depleted condition (DMEM), and Socs3 was further induced in the amino acid-depleted condition (1/5 DMEM) and by TGF-β1 treatment (Supporting Fig. 4A). HCV-RNA was similarly increased in these conditions (Supporting Fig. 4B). Foxo3a mRNA expression, as deduced from RTD-PCR, was increased up to 7-fold in the combination of amino acid depletion (1/5 DMEM), c-Jun overexpression, and TGF-β1 treatment (Supporting Fig. 4C). Socs3 mRNA expression was up-regulated by 8-fold in the same conditions (Supporting Fig. 4D). The promoter activity of Socs3 was significantly increased by amino acid depletion (1/5 DMEM) and TGF-β1 treatment (pGL4-SOCS3-WT, Supporting Fig. 4E), while mutation of the Foxo3a binding site in the Socs3 promoter (pGL4-SOCS3-MT) abrogated this regulation. These results confirmed that TGF-β signaling up-regulated the expression of Socs3 through the induction of Foxo3a.

TGF-β Signaling Suppresses mTORC1 Signaling. Previously, we demonstrated that malnutrition decreased mTORC1 and IFN signaling using Huh-7 cells and clinical samples.[6] In the present study, we examined the effect of TGF-β signaling on mTORC1 signaling. In Huh-7.5 cells and PHH, amino acid depletion (1/5 DMEM) repressed mTORC1 signaling, as demonstrated by the decreased expression of ras homolog enriched in brain (RHEB),[11] a stimulator of mTORC1 signaling, p-mTOR, and p-p70S6K (Fig. 5A). Interestingly, TGF-β1 further decreased this expression. The decreased mTORC1 signaling was independent of AMP-activated, alpha 1 catalytic subunit (AMPK), a suppressor of mTORC1 signaling, as the levels of p-AMPK were rather decreased by amino acid depletion (1/5 DMEM) and TGF-β1 treatment in Huh-7.5 cells and PHH (Fig. 5A). It could be speculated that TGF-β signaling, combined with malnutrition, repressed the expression of RHEB and induced the expression of Foxo3a, which leads to the impaired IFN signaling observed in the advanced fibrosis stage of CH-C (Fig. 5B). In the liver of CH-C

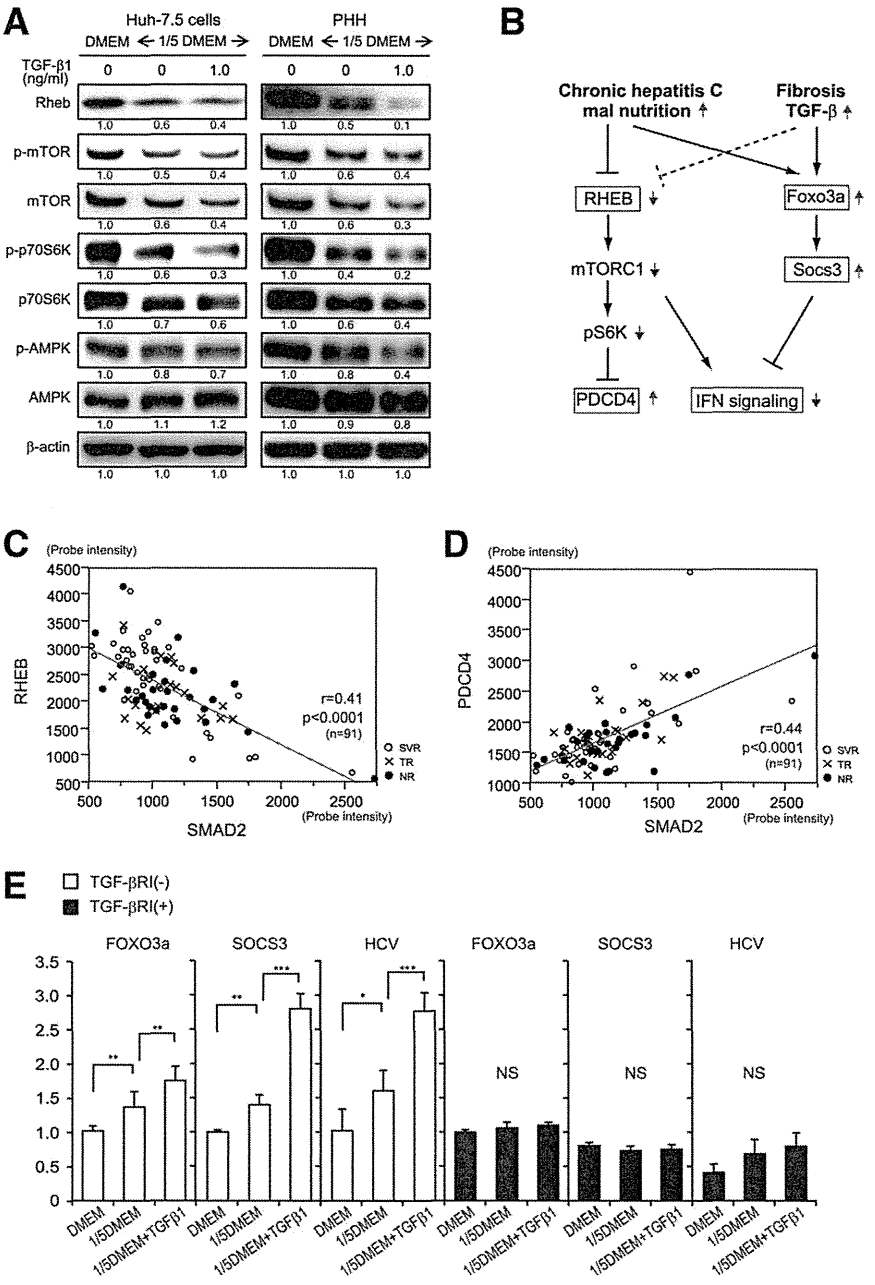

Fig. 5. TGF-β signaling represses mTORC1 signaling in Huh-7.5 cells, PHH, and the liver of CH-C patients. A: Western blotting of RHEB, mTOR, p70S8K, and AMPK in Huh-7.5 cells and PHH treated with amino acid depletion (1/5 DMEM) and TGF-β1. The experiments were repeated 3 times. B: Schematic representation of the effects of malnutrition and TGF-β signaling on IFN signaling. C,D: Significant correlations of Smad2 and RHEB (C), and Smad2 and PDCD4 (D) expression in the liver of CH-C patients. E: Blocking TGF-β signaling by TGF-β1 RI treatment abolishes the increase in Foxo3a, Socs3, and HCV replication by amino acid depletion (1/5 DMEM) and TGF-β1 treatment. The experiments were performed in triplicate and repeated 3 times ($*P < 0.05$, $**P < 0.01$, $***P < 0.001$).

patients, Smad2 expression was significantly negatively correlated with RHEB expression. The expression of programmed cell death 4 (PDCD4), which is negatively regulated by mTORC1 signaling at the transcriptional level (Fig. 5C),[12] was significantly positively correlated with Smad2 expression (Fig. 5D).

We further examined the effect of TGF-β1 on IFN signaling by using TGF-β RI. TGF-β RI substantially repressed the levels of p-Smad2 and p-Smad3 (Supporting Fig. 5). TGF-β RI abolished the induction of Foxo3a expression and the subsequent induction of Socs3 by amino acid depletion (1/5 DMEM) and TGF-β1 treatment (Fig. 5E). HCV replication in normal medium (DMEM), as deduced from *Gaussia* luciferase activity, was repressed by TGF-β RI, and the increase in HCV replication by amino acid depletion (1/5 DMEM) and TGF-β1 treatment was abrogated (Fig. 5E).

c-Jun Is Up-Regulated in the Liver of NR and Treatment-Resistant IL28B Minor Genotype Patients. We evaluated the clinical significance of c-Jun for treatment response. The expression of c-Jun was significantly higher in NR patients than in responder patients (SVR+TR) (Fig. 6A). Furthermore, c-Jun expression was significantly higher in patients with the treatment-resistant IL28B minor genotype

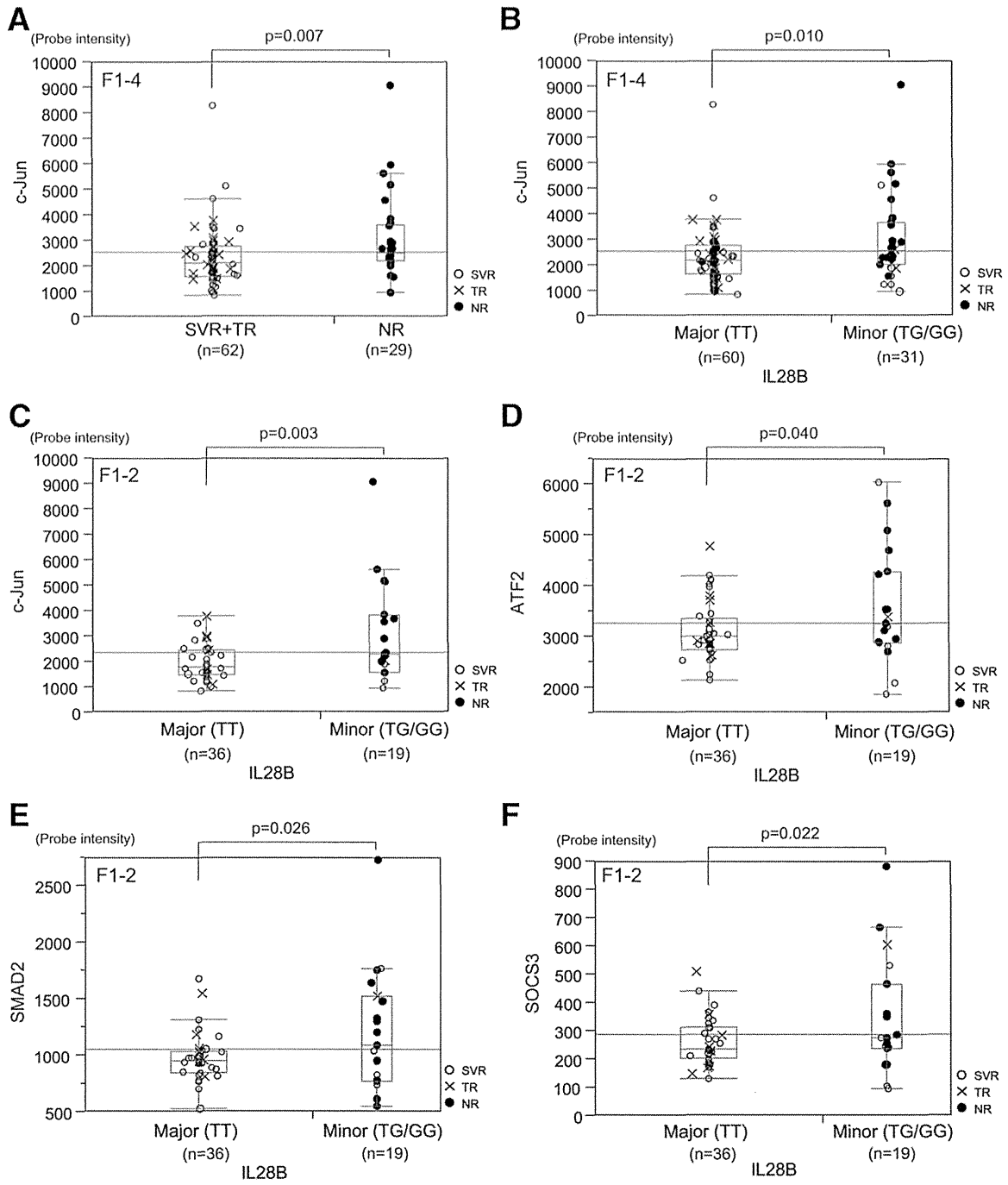

Fig. 6. Relationship between TGF-β signaling and treatment response and the IL28B genotype. The expression of c-Jun was up-regulated in NR (A) and IL28B minor genotype (TG/GG at rs8099917) (B) patients in all fibrosis stages (F1-4). The expression of ATF2 (D), Smad2 (E), and Socs3 (F) was up-regulated in IL28B minor genotype (TG/GG at rs8099917) patients at early fibrosis stages (F1-2).

(TG/GG at rs8099917) than in those with the treatment-sensitive IL28B major genotype (TT) (Fig. 6B).[5] Interestingly, TGF-β signaling was more activated in patients with the treatment-resistant IL28B minor genotype at an early stage of liver fibrosis (F1 and F2). The expression of c-Jun, ATF2, Smad2, and Socs3 was significantly higher in IL28B minor genotype patients (Fig. 6C-F).

BCAAs Inhibit TGF-β Signaling and Restore IFN Signaling. Previously, we reported that BCAAs restored IFN signaling in the amino acid-depleted condition (1/5 DMEM) by activating mTORC1 signaling and suppressing Foxo3a-Socs3 signaling.[6] In the present study, we examined whether BCAAs could inhibit TGF-β signaling and restore IFN signaling. Western